Supplementary Information for

Simultaneous Integration of Poly(dimethylsiloxane) Elastomer in Polymer Donor and Dimer Acceptor Enables Strain-Induced Power Enhancement in Intrinsically-Stretchable Organic Photovoltaics

*Jin-Woo Lee[†,a], Trieu Hoang-Quan Nguyen[†,a], Won Jung Kang[b], Soodeok Seo[a], Seungbok Lee[c], Seungjin Lee[d], Jaeyoung Choi,[a] Jimin Park[a], Jung-Yong Lee[c], Taek-Soo Kim[b], and Bumjoon J. Kim[a,]**

[a] Department of Chemical and Biomolecular Engineering, Korea Advanced Institute of Science and Technology (KAIST), Daejeon 34141, Republic of Korea

[b] Department of Mechanical Engineering, KAIST, Daejeon 34141, Republic of Korea

[c] School of Electrical Engineering, KAIST, Daejeon 34141, Republic of Korea

[d] Photoenergy Research Center, Korea Research Institute of Chemical Technology (KRICT), Daejeon, 34114, Republic of Korea

[*]All correspondence should be addressed to B. J. K. (E-mail: bumjoonkim@kaist.ac.kr)

Experimental Section

***Materials*:** 5-Bromo-2-thiophenecarboxylic acid, 4- dimethylaminopyridine (DMAP), and 1-(3-dimethylaminopropyl)-3-ethylcarbodiimide (EDC) were purchased from Tokyo Chemical Industry Co., Ltd. 2,5-bis(tributylstannyl)thiophene, tetrakis(triphenylphosphine)palladium (0) ($Pd(PPh_3)_4$), and all solvents were purchased from Sigma-Aldrich. Carbinol-terminated polydimethylsiloxanes (M_n = 1 kg mol^{-1}) was purchased from Gelest Inc. 3,9-Bis(2-butyloctyl)-12,13-bis(2-octyldodecyl)-12,13-dihydro-[1,2,5]thiadiazolo[3,4-e]thieno [2",3":4',5']thieno[2',3':4,5]pyrrolo[3,2-g]thieno[2',3':4,5]thieno[3,2-b]indole-2,10-dicarbaldehyde (Compound 1) was synthesized using similar approach to previous literature.[1-3] PM6-*b*-PDMS and DYBT were synthesized according to our previous literature,[4, 5] and the ^1H NMR spectra confirm the molecular structure. Poly[(9,9-bis(3′-((*N*,*N*-dimethyl)-*N*-ethylammonium)propyl)-2,7-fluorene)-*alt*-5,5′-bis(2,2′-thiophene)-2,6-naphthalene-1,4,5,8-tetracaboxylic-*N*,*N*′-di(2-ethylhexyl)imide]dibromide (PNDIT-F3N-Br) was synthesized according to the reported method.[6]

Synthesis of compound 2

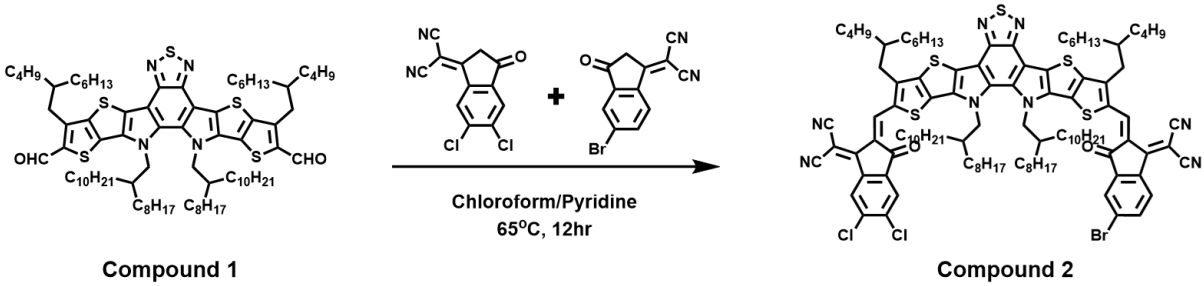

Scheme S1. Synthetic scheme for Compound 2.

INCN-Br-In (492 mg, 2.5 eq), INCN-2Cl (470 mg, 2.5 eq), and compound 1 (1000 mg, 1 eq) were added to a solvent mixture of chloroform (100 mL) and pyridine (4 mL). The reaction was placed in an oil bath at 65°C and stirred overnight. After the reaction, residual solvents were removed at low pressure (< 300 mbar), and the product was purified by silica-gel column chromatography using hexane/dichloromethane (1:1) as eluent to yield Y5-2Cl/Br-In as a black solid (380 mg, 28%).

^{1}H NMR (400 MHz, $CDCl_3$) δ 9.18 (d, J = 2.3 Hz, 2H), 8.80 (s, 1H), 8.58 (d, J = 8.4 Hz, 1H), 8.04 (d, J = 1.9 Hz, 1H), 7.96 (s, 1H), 7.87 (dd, J = 8.5, 2.0 Hz, 1H), 4.77 (d, J = 7.7 Hz, 4H), 3.19 (d, J = 7.5 Hz, 4H), 2.11 (dt, J = 13.4, 6.9 Hz, 4H), 1.39 (p, J = 6.4 Hz, 7H), 1.35 – 1.24 (m, 22H), 1.14 (qd, J = 7.6, 2.7 Hz, 24H), 1.06 – 0.95 (m, 32H), 0.91 – 0.75 (m, 32H)

Synthesis of DYBT

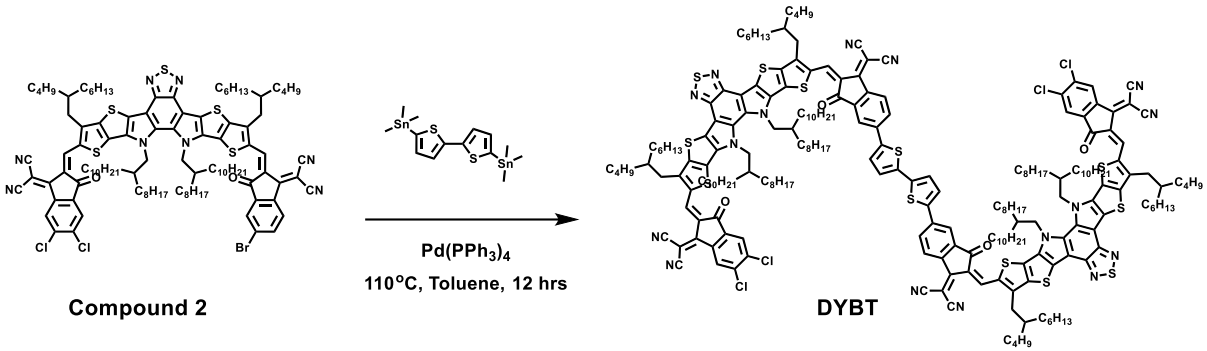

Scheme S2. Synthetic scheme for DYBT.

Under nitrogen protection, compound 3 (300 mg, 0.159 mmol), 5,5'-bis(trimethylstannyl)-2,2'-bithiophene (35.4 mg, 0.072 mmol), and $Pd(PPh_3)_4$ (3 mg, 0.0026 mmol) were dissolved in a 100 mL two-necked flask. Anhydrous toluene (30 mL) was added under the argon atmosphere. The mixture was reacted for 12 h at 110 °C. After removing residual solvents at low pressure (< 300 mbar) by a rotary evaporator, the product was purified by silica-gel column chromatography using hexane/ chloroform (1:4) as eluent to give DYBT as black solid (191 mg, 71%).

^{1}H NMR (500 MHz, Chloroform-d) δ 9.08 (s, 4H), 8.72 (d, J = 8.0 Hz, 4H), 7.86 (s, 4H), 7.72 (s, 2H), 7.52 (d, J = 6.0 Hz, 2H), 7.38 (s, 2H), 4.86 (s, 8H), 3.03 (d, J = 113.0 Hz, 8H), 2.26 (d, J = 10.1 Hz, 4H), 2.01 (d, J = 33.0)

Synthesis of compound 3

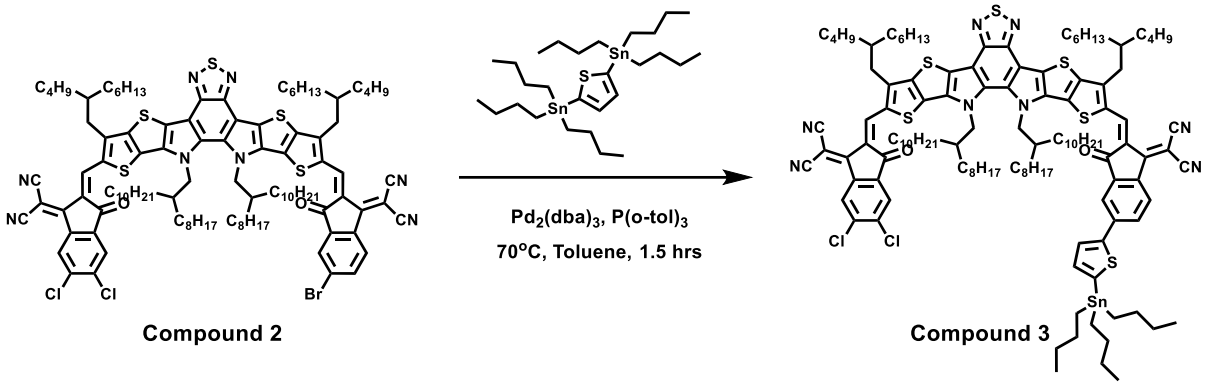

Scheme S3. Synthetic scheme for Compound 3.

Compound 3 was synthesized using similar approach to previous literature.[7] Under the protection of nitrogen, compound 2 (300 mg, 1 eq), 2,5-bis(tributylstannanyl)thiophene (8 eq, 0.20 mmol), $Pd_2(dba)_3$ (3 mg) and $P(o\text{-}tol)_3$ (6 mg) were dissolved in toluene (15 mL). After stirring at 70 °C for 1.5 h, the reaction mixture was allowed to cool to room temperature and then poured into methanol. The precipitate was collected by filtration and rinsed with ethanol to get crude product (280 mg). Compound 3 was used without further purification.

^{1}H NMR (400 MHz, $CDCl_3$) δ 9.17 (d, J = 8.6 Hz, 2H), 8.81 (s, 1H), 8.71 (d, J = 8.4 Hz, 1H), 8.14 (d, J = 1.8 Hz, 1H), 7.99 (dd, J = 8.4, 1.9 Hz, 1H), 7.68 (d, J = 3.4 Hz, 1H), 7.27 (d, J = 3.4 Hz, 1H), 4.76 (d, J = 7.9 Hz, 4H), 3.20 (d, J = 7.6 Hz, 4H), 2.11 (s, 5H), 1.54 (s, 10H), 1.51 (s, 5H), 1.39 (s, 6H), 1.25 (s, 15H), 1.00 (s, 18H), 0.87 (dd, J = 13.2, 6.3 Hz, 20H), 0.79 (ddd, J = 18.8, 9.3, 6.5 Hz, 21H), 0.67 (s, 2H), 0.46 (d, J = 3.6 Hz, 8H).

Synthesis of compound 4

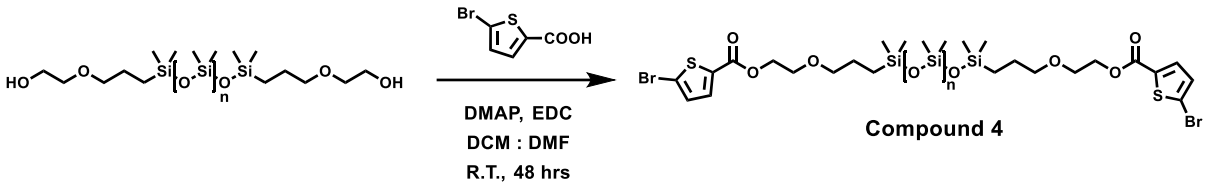

Scheme S4. Synthetic scheme for Compound 4.

To a solution of 5-bromo-2-thiophenecarboxylic acid (0.83 g, 1 eq), EDC (0.75 g, 1.2 eq), DMAP (0.17 g, 0.35 eq) in anhydrous CH_2Cl_2 (10 mL) and DMF (20 mL), carbinol-terminated polydimethylsiloxanes (1 g, 0.25 eq) was added. The reaction mixture was stirred at room temperature for 24 h. The mixture was then filtered and washed with CH_2Cl_2. The solvent was removed from the filtrate under vacuum. The crude product was purified with column chromatography on silica gel using n-hexane/CH_2Cl_2 (gradient from 10:0 to 7:3) as eluent to afford compound 4 as a pale-yellow oil (0.97 g, 83%).

^{1}H NMR (400 MHz, $CDCl_3$) δ 7.56 (d, J = 4.0 Hz, 2H), 7.06 (d, J = 4.0 Hz, 2H), 4.46 – 4.39 (m, 4H), 3.77 – 3.68 (m, 4H), 3.46 (t, J = 6.9 Hz, 4H), 1.62 (dt, J = 16.8, 7.0 Hz, 4H), 0.58 – 0.47 (m, 4H), 0.23 – -0.09 (m, 161H).

Synthesis of DYPDMS

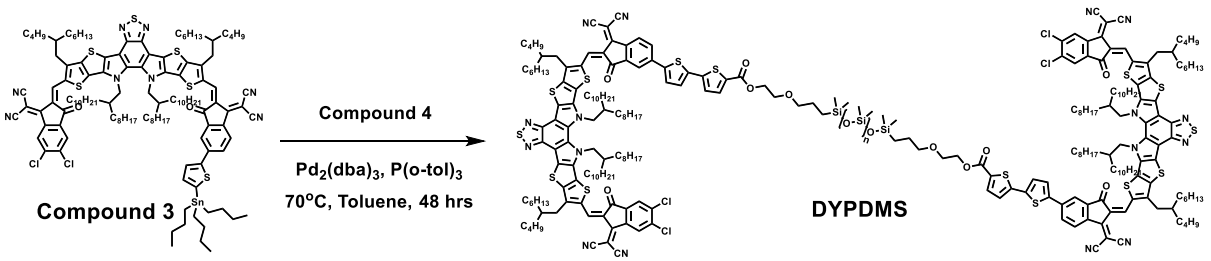

Scheme S5. Synthetic scheme for DYPDMS.

Under nitrogen protection, compound 3 (100 mg, 2eq), compound 4 (0.95 eq), $Pd_2(dba)_3$ (1 mg) and $P(o\text{-}tol)_3$ (2 mg) were dissolved in toluene (10 ml). After stirring at 70 °C for 48 h, the residual solvents were removed at low pressure (< 300 mbar), and the product was purified by silica-gel column chromatography using hexane/ethyl acetate (9:1) as eluent. The obtained product was further washed with hexane to remove unreacted PDMS to yield DYPDMS as a dark green solid (78.9 mg, 69%).

^{1}H NMR (500 MHz, Chloroform-d) δ 9.16 (s, 4H), 8.79 (s, 2H), 8.72 (s, 2H), 8.24 – 7.87 (m, 6H), 7.75 (d, J = 7.7 Hz, 2H), 7.49 (s, 2H), 7.34 (s, 2H), 7.22 (s, 2H), 4.79 (s, 8H), 4.47 (d, J = 5.2 Hz, 4H), 3.77 (t, J = 5.0 Hz, 4H), 3.50 (t, J = 6.9 Hz, 4H), 3.29 – 3.03 (m, 8H), 2.13 (s, 13H), 1.65 (s, 5H), 1.55 (s, 19H), 1.24 (s, 60H), 1.12 (d, J = 19.5 Hz, 55H), 1.02 (s, 85H), 0.90 – 0.70 (m, 73H), 0.60 – 0.48 (m, 5H), 0.08 – 0.06 (m, 63H).

Synthesis of compound 5

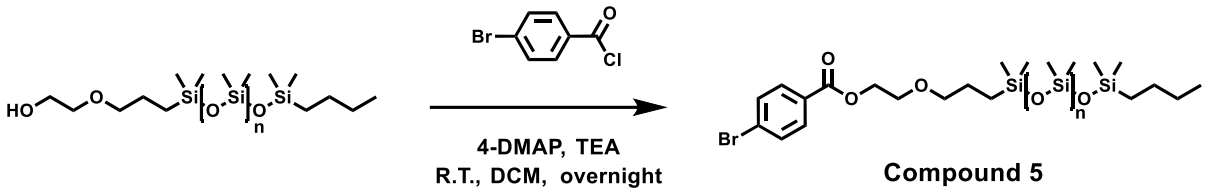

Scheme S6. Synthetic scheme for compound 5.

The hydroxy group-ended PDMS (2 g, 0.11 mmol) was dissolved in 20 mL of DCM in a 50 mL one neck round-bottom flask. In the other 100 mL two neck round-bottom flask, 4-bromobenzoyl chloride (219 mg, 1 mmol), triethylamine (TEA, 61 mg, 0.6 mmol), and 4-dimethylaminopyridine (4-DMAP, 13 mg, 0.1 mmol) were dissolved in the 20 mL of DCM. The PDMS solution was dropwise added into the 100 mL flask under the nitrogen atmosphere and stirred overnight at room temperature. The mixture was purifed by silica packed column chromatography using chloroform: hexane (7:1) mixture. The purified compound 5 was obtained as a slightly yellowish liquid (1.2 g, 55%).

^{1}H NMR (500 MHz, chloroform-d): δ (ppm) 7.95 (d, 2 H), 7.60 (d, 2 H), 4.50 (m, 2H), 3.80 (m, 2 H), 3.50 (m, 2 H), 0.10 (m, 841 H).

Synthesis of PM6-b-PDMS

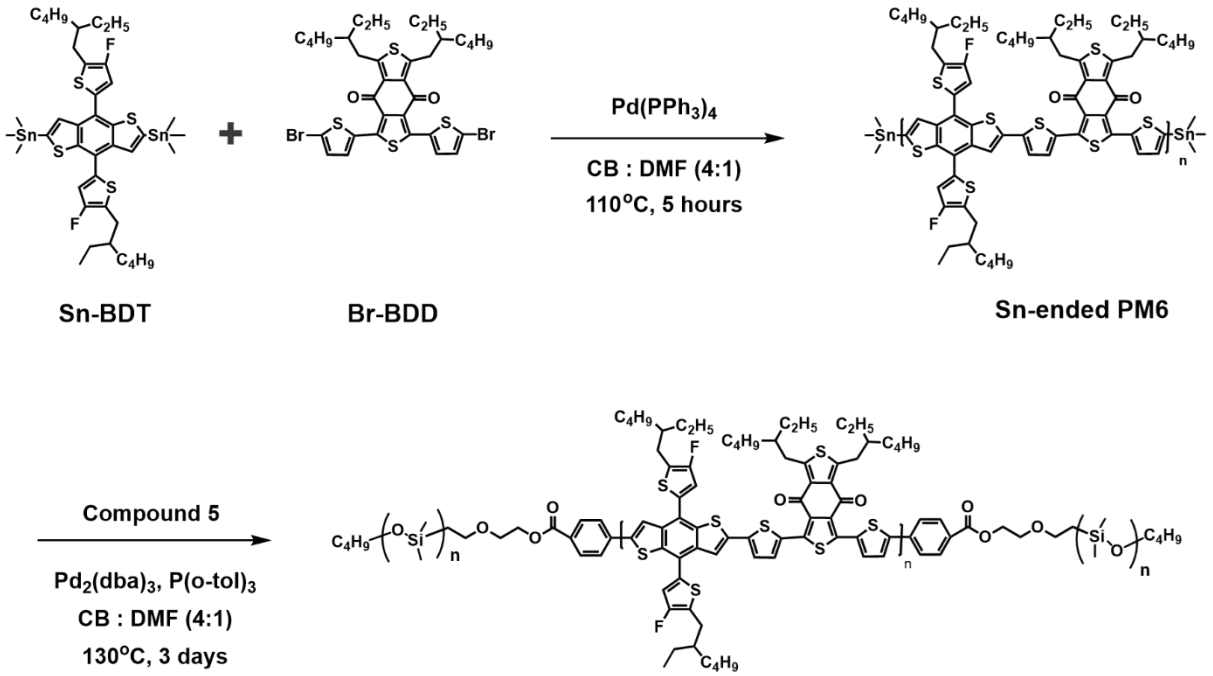

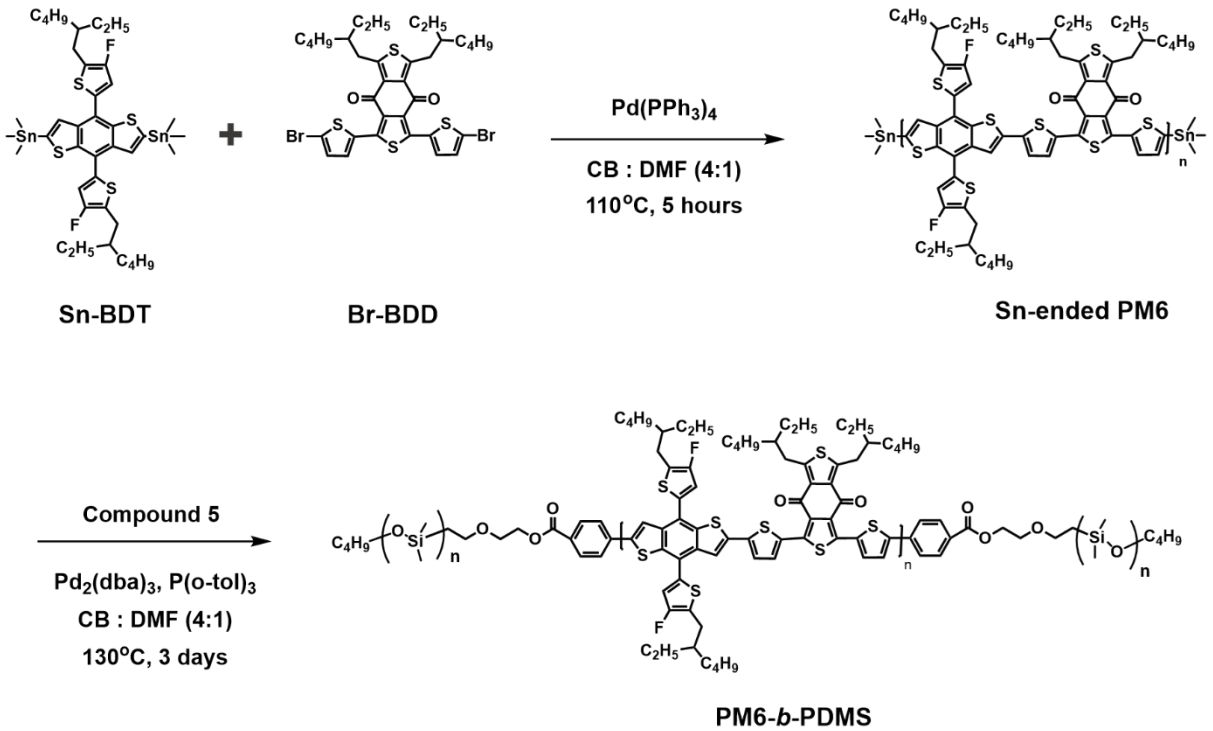

Scheme S7. Synthetic scheme for PM6-*b*-PDMS.

Sn-BDT (450 mg, 0.47 mmol) monomer, Br-BDD (333 mg, 0.43 mmol) monomer, and $Pd(PPh_3)_4$ (15 mg, 0.02 mmol) were added in a 20 mL vial. After purging with argon gas 3 times, a mixture of 12 mL of chlorobenzene (CB) and 3 mL of *N*,*N*-dimethyforamide (DMF) was added into the vial. The mixture was reacted for 5 h at 110 ºC. The mixture was precipitated in methanol and purified by soxhlet extraction by methanol, acetone, hexane, and chloroform (CF). Then, the polymer in the CF fraction was precipitated in methanol (390 mg, 73%).

Subsequently, Sn-ended PM6 (100 mg), compound 5 (50 mg), $Pd_2(dba)_3$ (10 mg, 10.92 μmol), and $P(o\text{-}tol)_3$ (22 mg, 71 μmol) were combined in a 20 mL vial. The excess amount of compound 5 relative to Sn-ended PM6 was added to improve the reactivity. After purging with argon gas for 3 times of 5 min, 8 mL of CB and 2 mL of DMF were added. The mixture was stirred for 3 days at 130 ºC. The mixture was precipitated in methanol and purified by soxhlet extraction by methanol, acetone, hexane, and chloroform (CF). Since the PDMS homopolymers have high solubilities in hexane, Soxhlet purification using hexane was performed for 1 day to remove unreacted PDMS homopolymers. The purified polymers were precipitated in methanol and washed with acetone and hexane sequentially to remove the residual salt and PDMS polymers. Then, the polymers were dried under vacuum.

^{1}H NMR (1,2-dichlorobenzene-d_4, 395 K, 500 MHz): 7.85 (br, aromatic protons), 7.45 (br, aromatic protons), 7.33 (br, aromatic protons), 3.45 (br), 2.96 (br), 1.82-1.30 (br, aliphatic protons), 1.25-0.90 (br, aliphatic protons), 0.20-0.18 (br, protons attached to PDMS chain).

Characterizations: Bruker AVANCE NEO (11.74 T) 500 MHz spectrometer was used to measure ^{1}H NMR spectra. The chemical shifts in the spectra have units of ppm. Bruker Autoflex MALDI-ToF mass spectrometer was used to measure the molecular weights of the DSMAs. Number-average molecular weight (M_n) and dispersity ($Đ$) of the PDMS and DYPDMS were determined by size exclusion chromatography (SEC) analyses in 1,2-dichlorobenzene at 80 °C, calibrated with polystyrene standards. M_n and $Đ$ of PM6 and PM6-*b*-PDMS were determined by SEC analyses in 1,2,4-trichlorobenzene at 100 °C, calibrated with polystyrene standards. UV-1800 spectrophotometer was used for the ultraviolet-visible (UV−Vis) absorption spectra. The differential scanning calorimetry (DSC) profiles were obtained by TA Instruments DSC 25 with heating rates of 5 °C min^{-1} from 20 to 330 °C. Cyclic voltammetry (CV) was performed using an EG and G Parc model 273 Å potentiostat/galvanostat system in a 0.1 M tetrabutylammonium perchrolate solution with nitrogen degassed anhydrous acetonitrile as the supporting electrolyte, at a scan rate of 50 mV s^{-1}. A glassy carbon electrode was used as the working electrode. A platinum wire was used as the counter electrode, and an Ag/AgCl electrode was used as the reference electrode. The redox couple ferricenium/ferrocene was used as external standard. The highest occupied molecular orbital (HOMO) and lowest unoccupied molecular orbital (LUMO) energy levels were estimated from CV: E_{HOMO} (eV) = −($E_{onset}^{ox.}$ − $E_{onset}^{Fc/Fc+}$) + E_{HOMO}^{Fc}; E_{LUMO} (eV) = − ($E_{onset}^{red.}$ − $E_{onset}^{Fc/Fc+}$) + E_{HOMO}^{Fc}; $E_{onset}^{Fc/Fc+}$ = 0.44 eV, E_{HOMO}^{Fc} = −4.8 eV. The atomic force microscopy (AFM) images were measured by NX10 from Park Systems. Grazing incidence wide-angle X-ray scattering (GIXS) analysis was conducted at the Pohang Accelerator Laboratory (beamline 3C, Republic of Korea), with incidence angles between 0.12 − 0.14°. The resonant soft X-ray scattering (RSoXS) experiment was performed at beamline 11.0.1.2 in the S11 Advanced Light Source (United States). Blend films for the RSoXS measurement were prepared on a 100 nm-

thick, 1.0 mm × 1.0 mm Si_3N_4 membrane supported by a 200-μm thick, 5 mm × 5 mm silicon frame (Norcada Inc.). The optimized molecular structures were calculated by density functional theory (DFT) method with the B3LYP function and the 6-31G* basis set using a modelling software (Spartan'14).

OSC Fabrication and Characterization: The OSCs with a normal architecture (indium tin oxide (ITO)/ poly(3,4-ethylenedioxythiophene):poly(styrenesulfonate) (PEDOT:PSS)/active layer/PNDIT-F3N-Br/Ag) were prepared with the following procedures. ITO-coated glass substrates were treated by ultrasonication with deionized water, acetone, and isopropyl alcohol. Then, the ITO substrates were dried for 6 h in an oven (70 °C) at an ambient pressure, and then plasma treated for 10 min. Spin-coating of the PEDOT:PSS solution (Clevios, AI4083) was performed at 3000 rpm for 30 s onto the ITO substrates, then the substrate/film was annealed in air (150 °C, 15 min) before transferring into an N_2-filled glovebox. The active layer solutions were dissolved together in chlorobenzene with an optimized condition (donor:acceptor blend ratio of 1.0:1.2 w/w, a total concentration of 20 mg mL^{-1}, and 3,5-dichlorobromobenzene as a solid additive at a concentration of 10mg/mL), and then stirred on a 90 ℃ plate during overnight. To compare the effects of physical mixing and chemical bonding of PDMS in acceptor blends, DYBT:PDMS was prepared with a weight ratio of 4:1, while DYBT:DYPDMS was prepared with a weight ratio of 3:2. The solution was spin-coated onto the ITO substrates/ PEDOT:PSS samples to form active layers with a thickness of ~150 nm. Then, the samples were annealed at 80 ℃ for 10 min and dried with high vacuum (< 10^{-6} torr) for 1 h. PNDIT-F3N-Br in methanol (1 mg mL^{-1}) was then spin-coated with the condition of 3000 rpm for 30 s. Finally, Ag (100 nm) was deposited under high vacuum (~10^{-6} Torr) in an evaporation chamber. Optical microscopy (OM) was used to measure the exact photoactive

area of the mask (0.04 cm^2). Keithley 2400 SMU instrument was used to measure the power conversion efficiencies (PCEs) under an Air Mass 1.5 G solar simulator (100 mW cm^{-2}, solar simulator: K201 LAB55, McScience), satisfying the Class AAA, ASTM Standards. K801SK302 of McScience was used as a standard silicon reference cell to calibrate the exact solar intensity. K3100 IQX, McScience Inc. instrument was used to analyze the external quantum efficiency (EQE) spectra, equipped with a monochromator (Newport) and an optical chopper (MC 2000 Thorlabs).

Space-Charge-Limited Current (SCLC) Mobility Measurements: Hole and electron mobilities of pristine constituents and blend films were measured by SCLC method using device structures of ITO/PEDOT:PSS/active layers/Au (hole-only) and ITO/ZnO/polymer blends/Ca/Al (electron-only). A range of voltage from 0 to 6 V was applied for the current-voltage measurements, and the results were fitted by the Mott-Gurney law.

$$J = \frac{9\varepsilon_0\varepsilon_r\mu_0 V^2}{8L^3}$$

where J is the current density, ε_0 is the permittivity of free space (8.85×10^{-14} F cm^{-1}), ε_r is the relative dielectric constant of the transport medium (active layer), μ_0 is the charge carrier (hole or electron) mobility, V is the potential across the device ($V = V_{applied} - V_{bi} - V_r$, where V_{bi} is the built-in potential and V_r is the voltage drop caused by the resistance), and L is the thickness of the blend or pristine films. The hole and electron mobilities can be calculated from the slope of the $J^{1/2}$–V curves.

Thermal Stability Test of OSCs: To assess the morphological stability of photoactive layers under thermal stress and prevent degradation of electron-transporting layers and electrodes, we pre-annealed devices before depositing the electron-transporting layers. Substrates with a

Glass/PEDOT:PSS/photoactive layer structure were annealed at 80 ºC in a vacuum chamber for 0–500 h. Subsequently, PNDIT-F3N-Br and Ag electrode layers were deposited using the same fabrication procedures as above. Photovoltaic performance was then measured following the same protocol, depending on annealing times.

Pseudo Free-Standing Tensile Test: In the pseudo free-standing tensile method, the films were prepared with the same condition as the OSC fabrications. The films were spin-casted onto the polystyrene sulfonic acid (PSS)-coated glass substrate, and cut into a dog-bone shape by a femtosecond laser. Then, the films were floated onto the water surface, and attached to the grips by van der Waals forces. The strain was applied at a fixed strain rate (0.8×10^{-3} s^{-1}), and the tensile load values were measured by a load cell with high resolution (LTS-50GA, KYOWA, Japan). Elastic modulus was calculated using the least square method for the slope of the linear region of the stress-strain curve within 1 % strain.

Intrinsically Stretchable Organic Solar Cell (IS-OSC) Fabrication: Normal-type IS-OSCs with a device configuration of thermoplastic polyurethanes (TPU)/modified PH1000/AI4083/photoactive layers/PNDIT-F3N-Br/eutectic gallium indium (EGaIn) were fabricated. The modified PH1000 solution was prepared to contain 5 vol% of dimethyl sulfoxide (DMSO) in order to enhance the electrical conductivity of PH1000, 2 vol% of polyethylene glycol to improve its mechanical stretchability, and 0.5 vol% of Zonyl fluoro surfactant (FS-30) to boost the surface wettability. This solution was then spin-coated onto the plasma-treated TPU substrate at 1200 rpm for 40 s and subsequently baked for 20 min at 100 °C in air. Afterward, an AI4083 hole transporting layer with 0.5 vol% FS-30 was spin-coated at 2500 rpm for 40 s onto the PH1000/TPU substrate and dried at 100 °C for 20 min. The

photoactive layers were then spin-coated under the same conditions used for the OSC fabrication on the rigid ITO/glass substrate. Then, the PNDIT-F3N-Br solution in methanol at a concentration of 1 mg mL^{-1} was spin-coated at 3000 rpm for 40 s, forming a 5 nm thick electron transporting layer on the active layer. Finally, EGaIn liquid metal was sprayed on the layer through a deposition mask. The photovoltaic performance of IS-OSCs was assessed using the same equipment utilized for evaluating the performance of the rigid OSCs.

PowerOutput Evaluation of the IS-OSCs at Different Strains: To estimate the changing power output of IS-OSCs at increasing strain values, we employed the following assumptions and methods: 1) Despite EGaIn deposited by spray-coating lacking perfectly defined edge boundaries, we assumed the shape of the EGaIn to be rectangular for simplified calculations. Thus, areal changes in IS-OSCs were calculated by multiplying changed length and height of EGaIn. 2) Accurate performance evaluation of IS-OSCs requires a fixed area mask; therefore, we used the same mask area (0.04 cm^2) for all PCE evaluations of IS-OSCs. 3) We confirmed that the variation in PCE due to mask areas ranging from 0.04 to 0.1 cm^2 is very marginal; hence, we calculated the normalized power output values at given strains by multiplying the normalized PCE values, measured using a 0.04 cm^2 mask, with the estimated normalized area.

Supplementary Figures & Tables

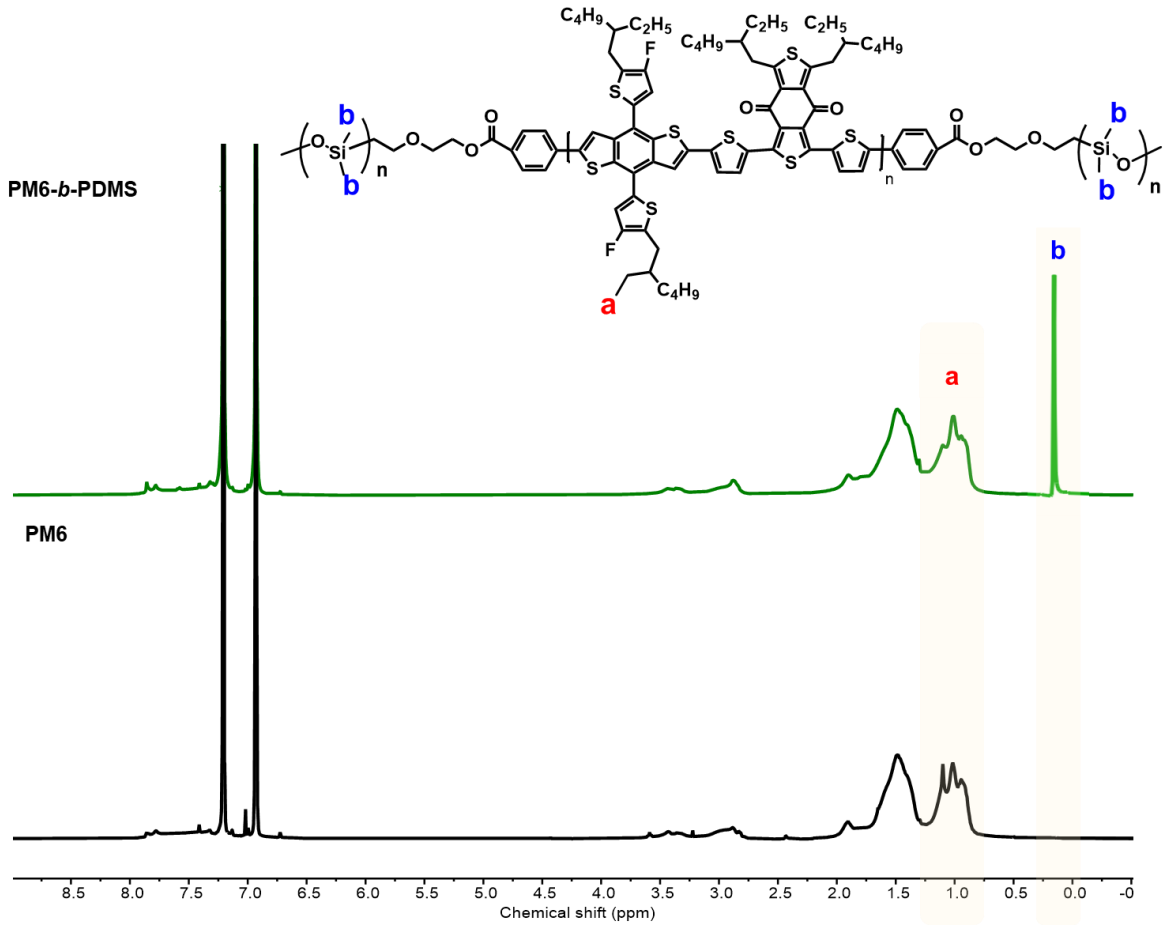

Fig. S1. ^{1}H NMR spectrum of PM6-*b*-PDMS and PM6.

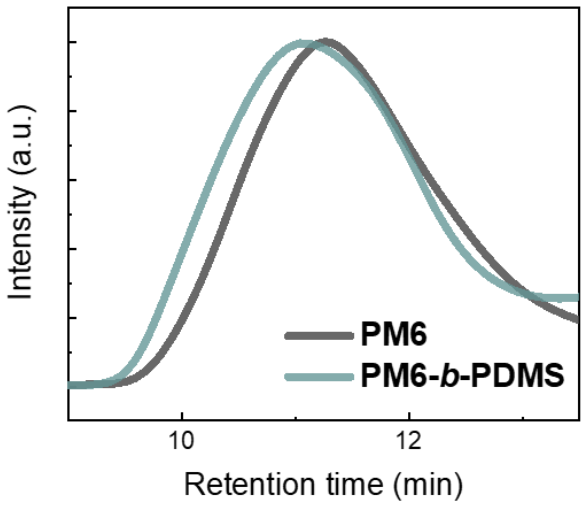

Fig. S2. SEC profiles of PM6 and PM6-*b*-PDMS.

Table S1. Molecular weight information of pristine PDMS polymer, and DYPDMS measured by SEC 100°C using 1,2,4-trichlorobenzene as eluent.

Polymer	M_n (kg mol^{-1})	$Đ$
PM6	134	2.6
PM6-*b*-PDMS	164	3.0

Table S2. Integrated peak area from the ^{1}H NMR spectra and estimated numbers of PDMS units per polymer chain derived from NMR and SEC data.

Polymer	$A^{R\ a)}$	$A^{PDMS\ b)}$	$Num^{PDMS\ c)}$
PM6	1.0	0.00	0.0
PM6-*b*-PDMS	1.0	0.48	1.5

[a)]The integrated value of the alkyl region from 0.90 to 1.25 ppm in the ^{1}H NMR spectra, normalized to 1 for comparison. [b)]The integrated value from 0.18 to 0.20 ppm in the ^{1}H NMR spectra, corresponding to the PDMS fraction, compared against the alkyl fraction. [c)] The number of PDMS blocks per PM6 block, calculated using both SEC and NMR results.

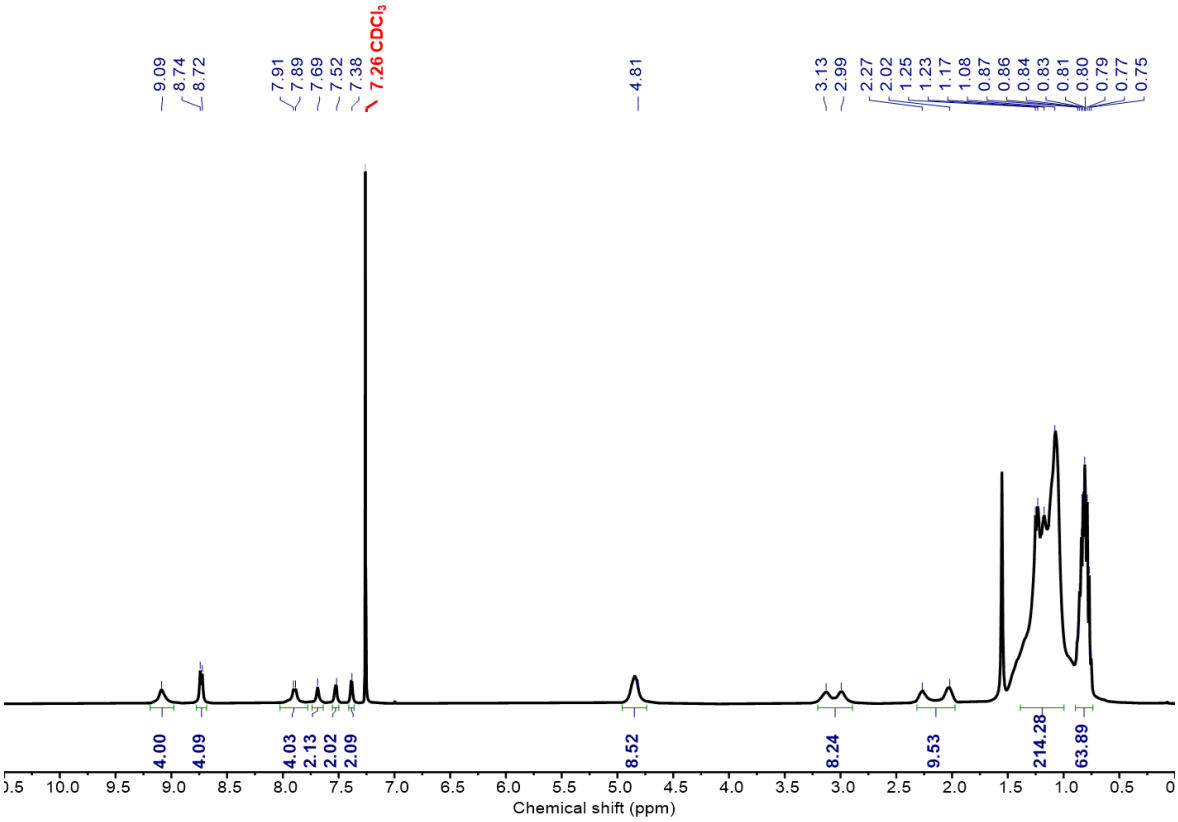

Fig. S3. ^{1}H NMR spectrum of DYBT.

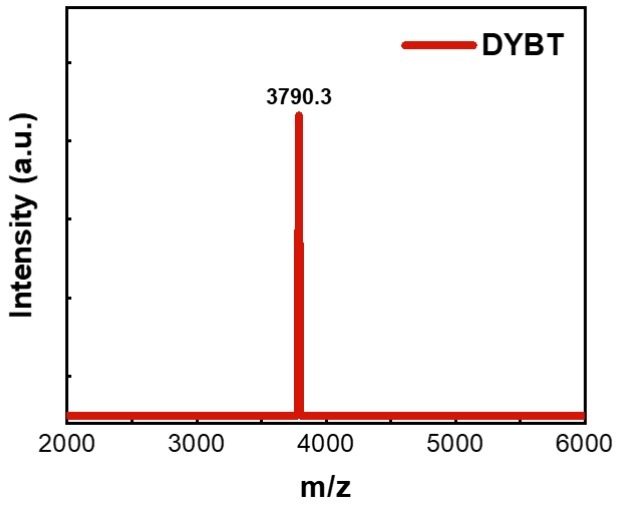

Fig. S4. MALDI-ToF spectra of DYBT.

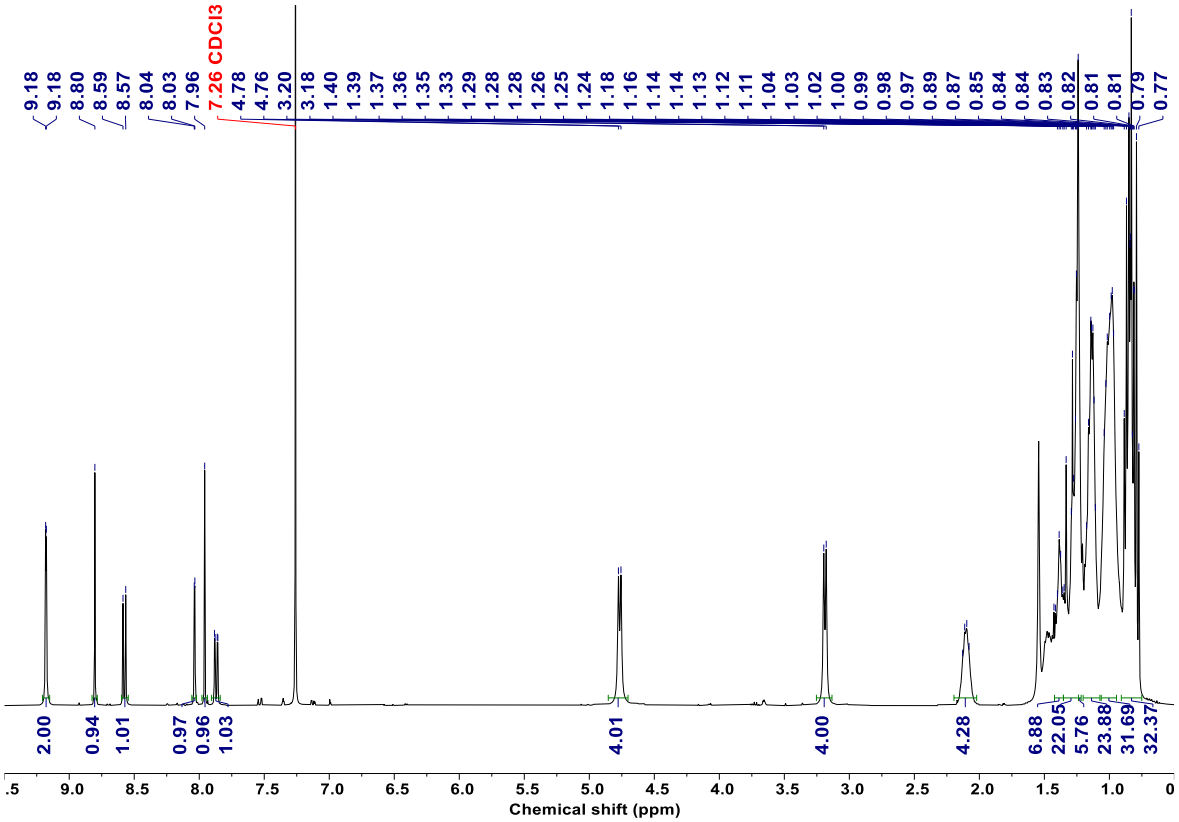

Fig. S5. ^{1}H NMR spectrum of compound 2.

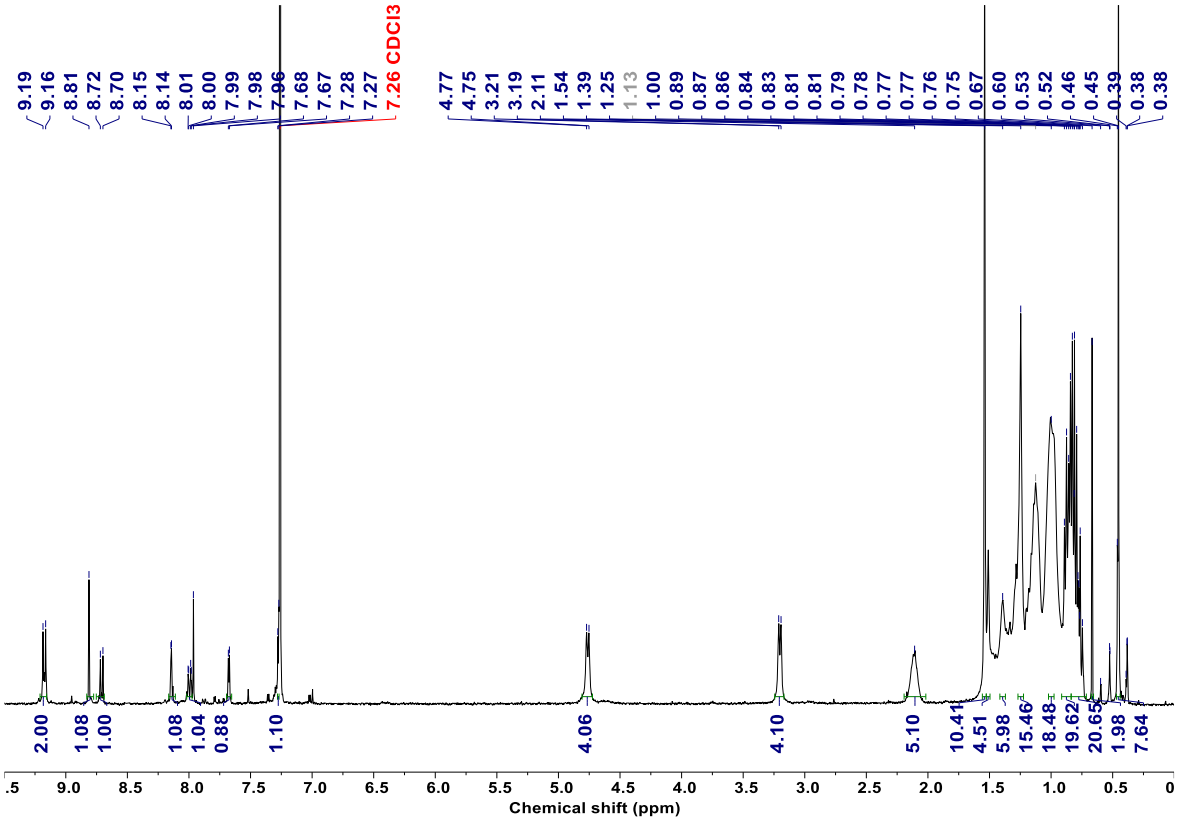

Fig. S6. ^{1}H NMR spectrum of compound 3.

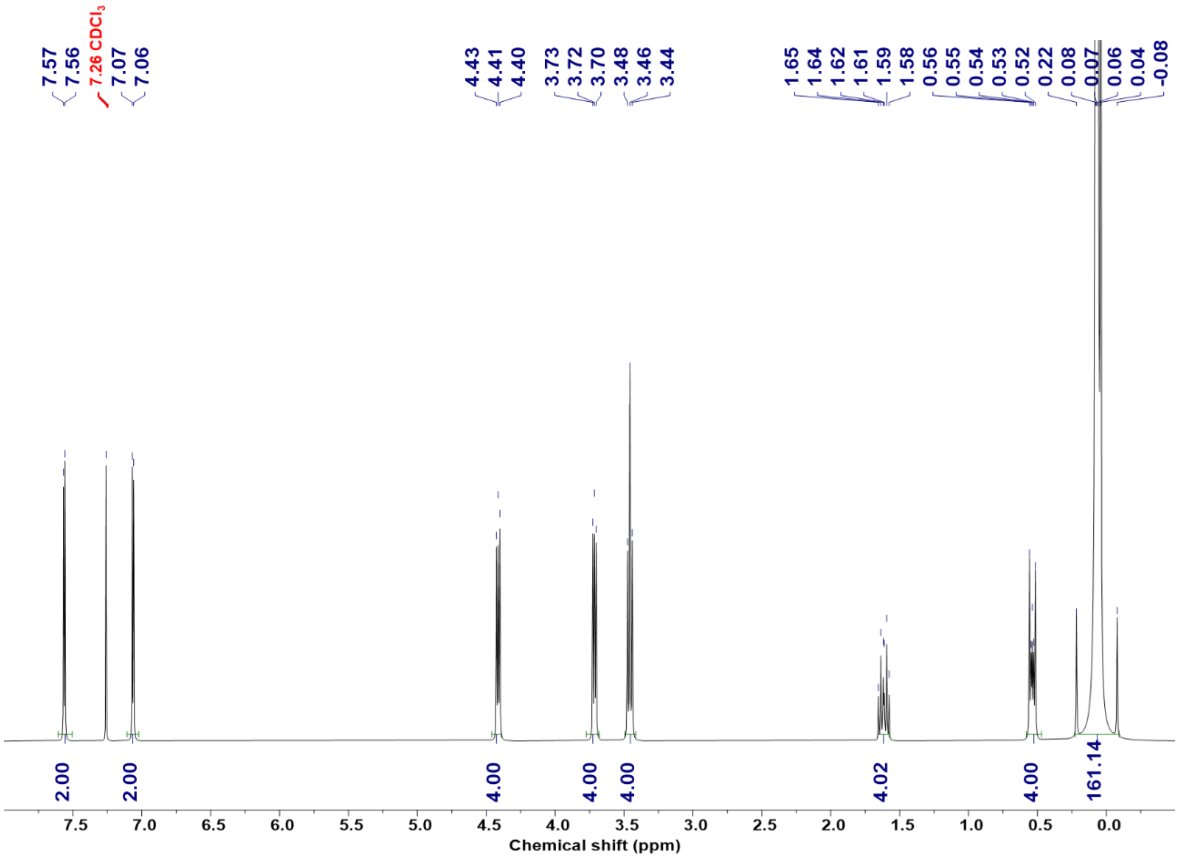

Fig. S7. ^{1}H NMR spectrum of compound 4.

Table S3. Molecular weight information of Pristine PDMS polymer, and DYPDMS measured by SEC at 80 °C using 1,2-dichlorobenzene as eluent.

Polymer	M_n (kg mol^{-1})	$Đ$
Pristine PDMS	1.0	2.5
DYPDMS	5.2	1.2

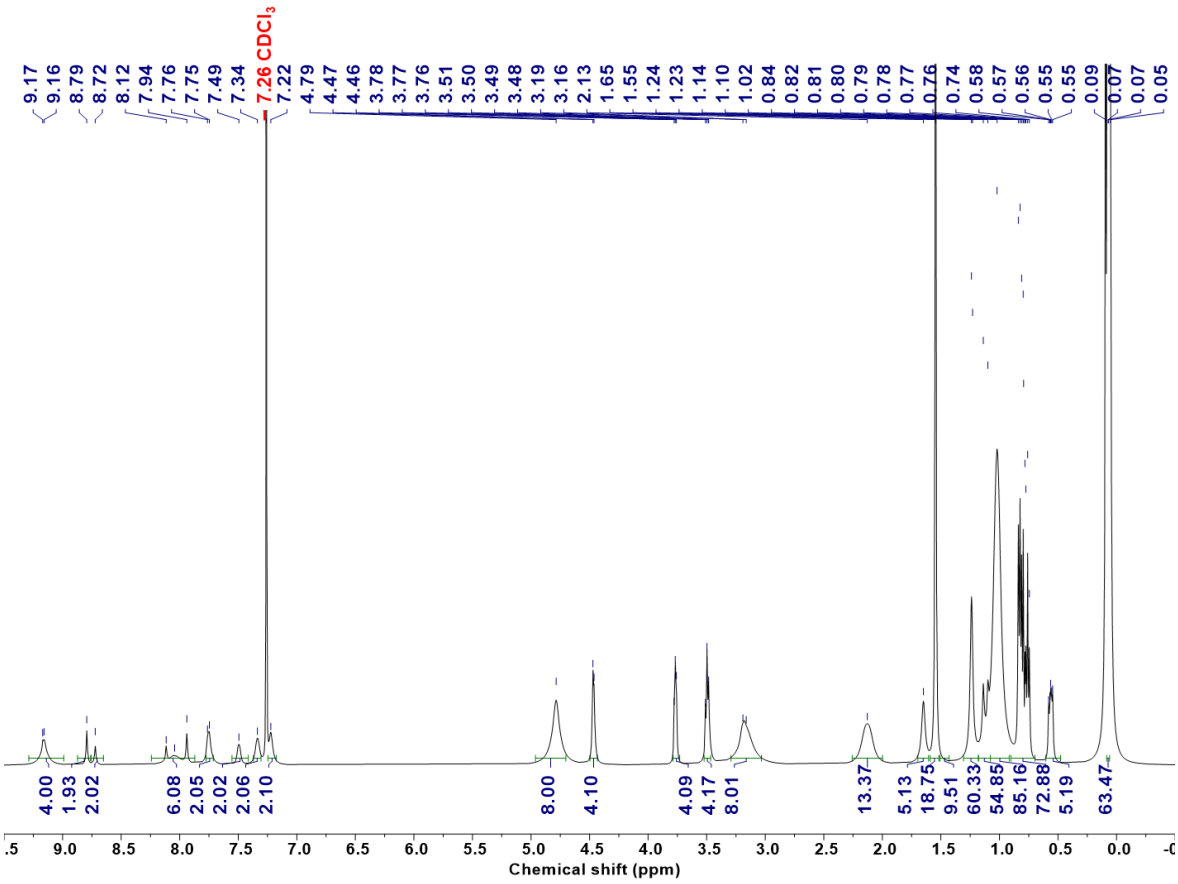

Fig. S8. ^{1}H NMR spectrum of DYPDMS.

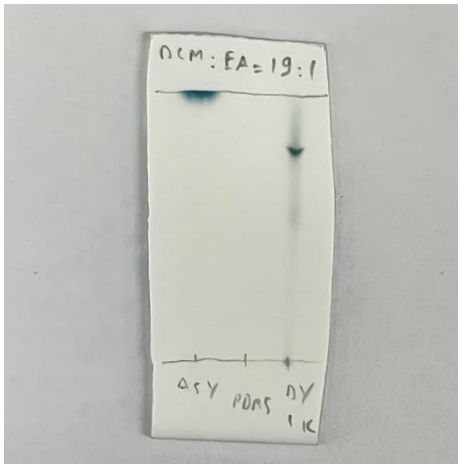

Fig. S9. TLC plate of compound 2 (left), pristine PDMS (middle), DYPDMS (right).

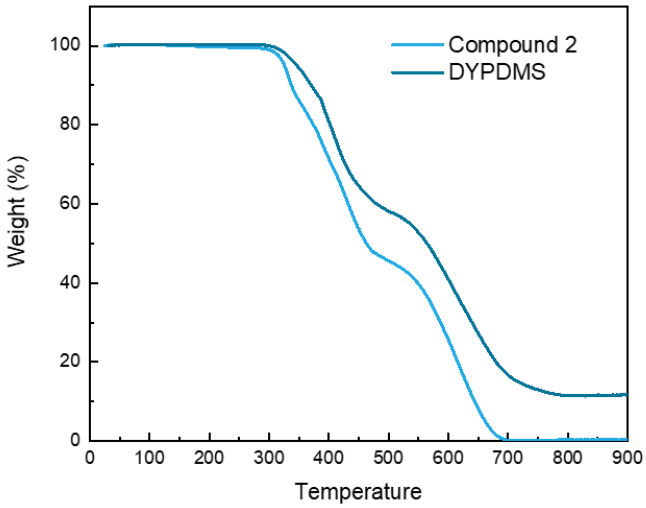

Fig. S10. TGA spectra of compound 2 and DYPDMS.

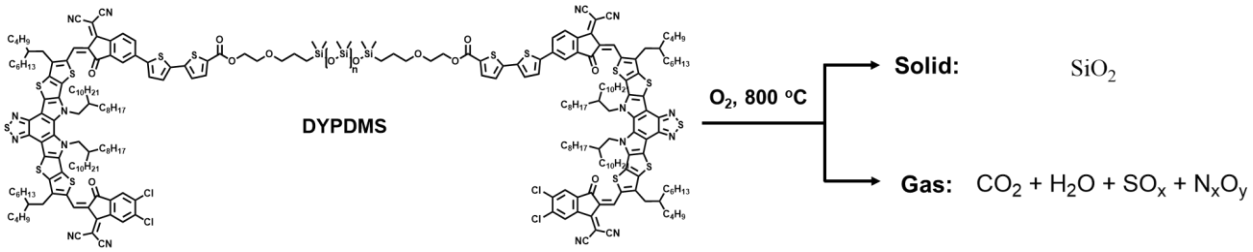

Fig. S11. Thermo-oxidative degradation of DYPDMS.

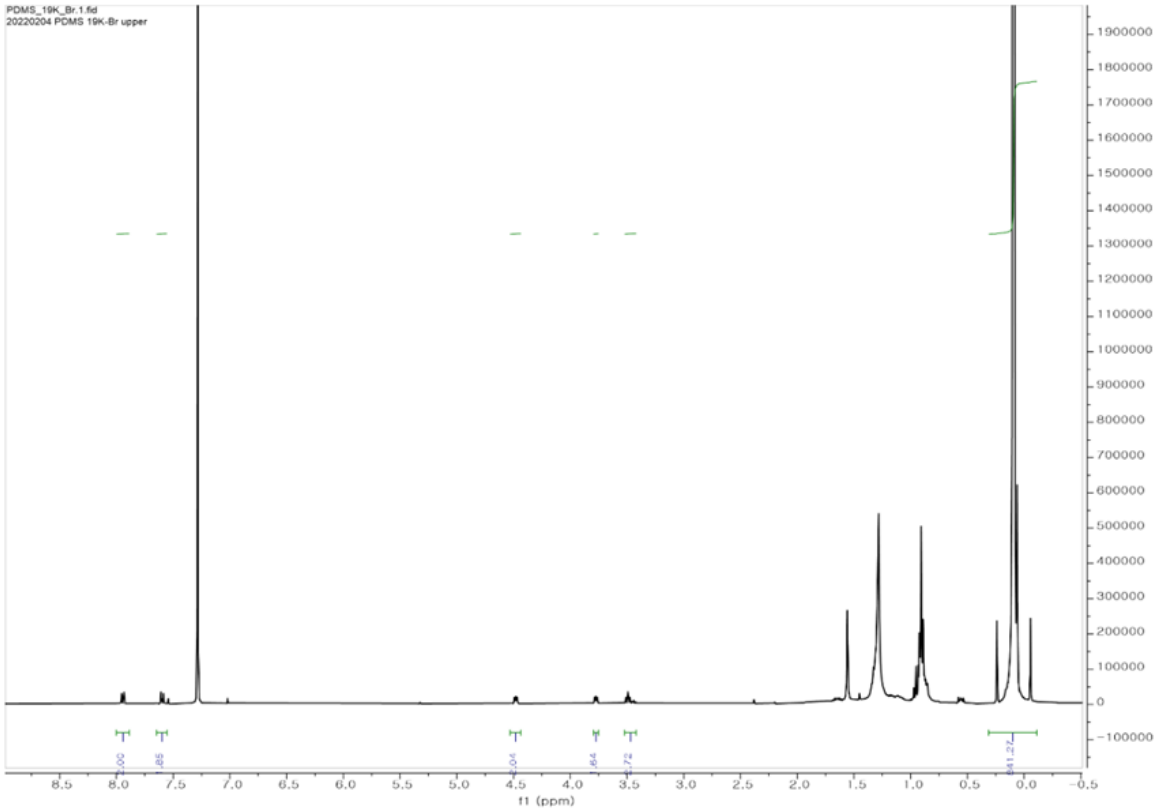

Fig. S12. ^{1}H NMR spectrum of compound 5.

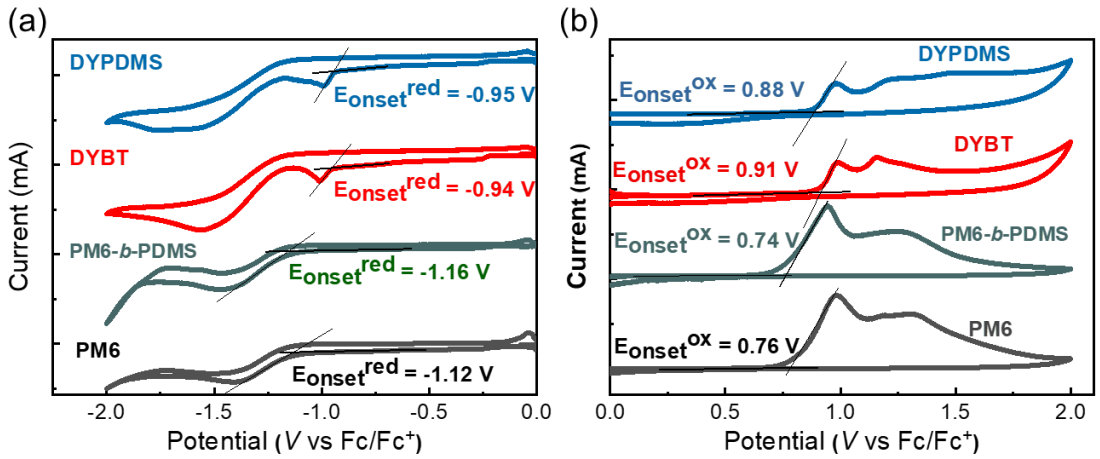

Fig. S13. Cyclic voltammograms for (a) reduction and (b) oxidation cycles of photoactive materials.

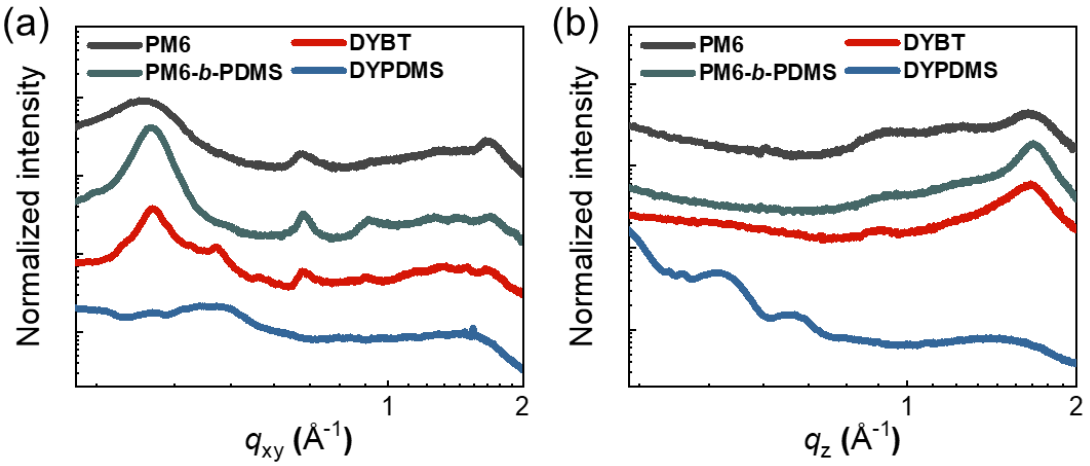

Fig. S14. GIXS linecut profiles of pristine constituents in the (a) IP and (b) OOP directions.

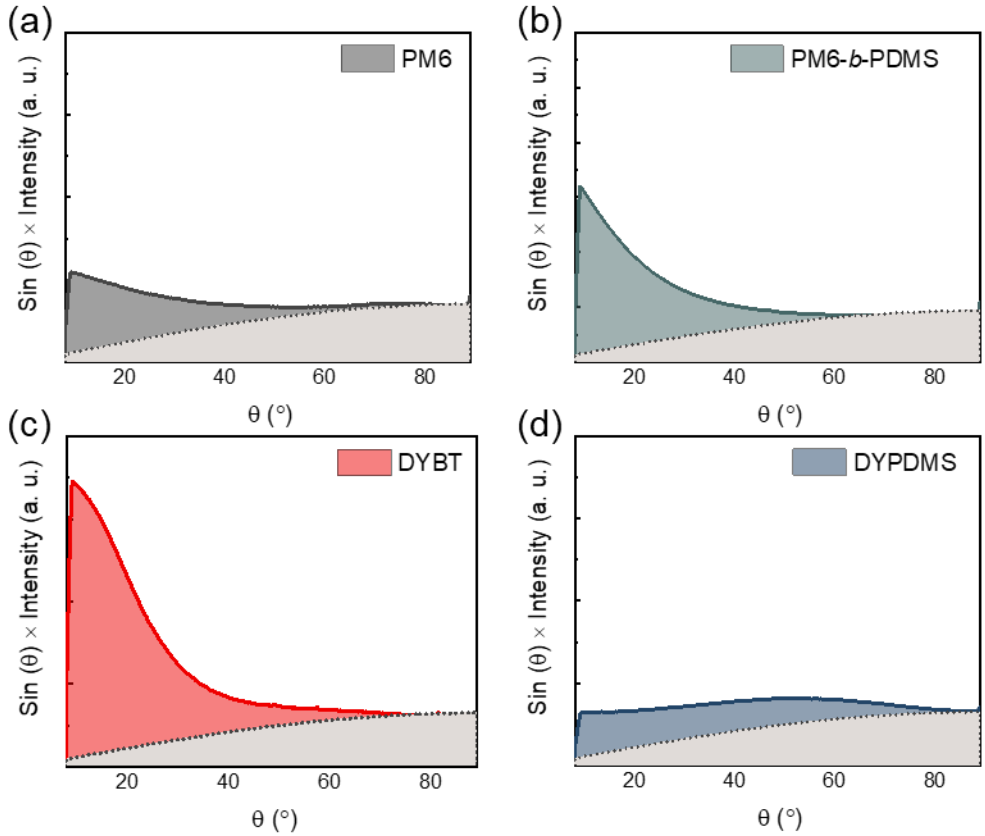

Fig. S15. Pole figures of (a) PM6, (b) PM6-*b*-PDMS, (c) DYBT, and (d) DYPDMS acquired at (010) scattering peaks using GIWAXS linecut profiles.

Table S4. Crystalline parameters for IP (100) and OOP (010) scattering peaks of the pristine constituents estimated from GIXS linecut profiles.

Material	$d_{(100)}^{IP}$ (Å)	$L_{c\ (010)}^{IP}$ (nm)	$d_{(010)}^{OOP}$ (Å)	$L_{c\ (010)}^{OOP}$(nm)
PM6	22.3	7.6	3.8	2.5
PM6-*b*-PDMS	21.7	12.6	3.8	3.4
DYBT	21.0	15.8	3.9	3.0
DYPDMS	–	–	4.5	0.8

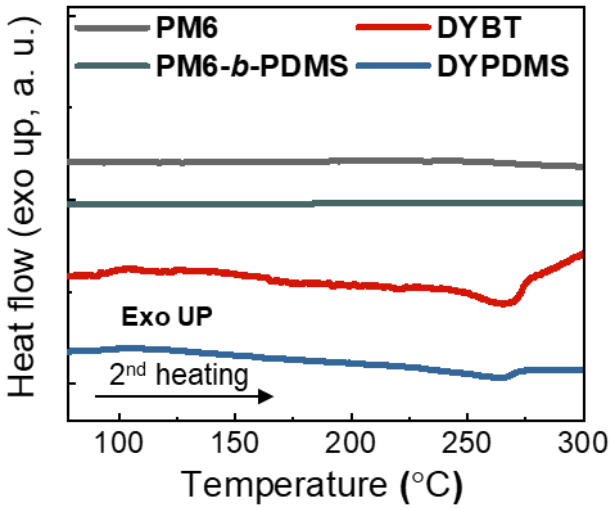

Fig. S16. DSC 2nd heating profiles of the photoactive materials (exo up).

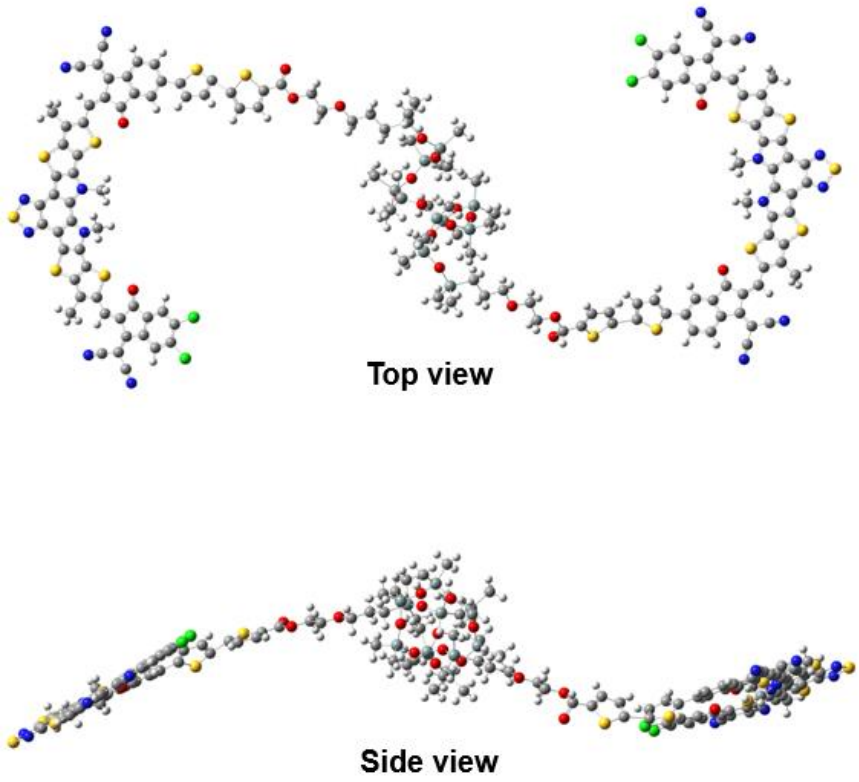

Fig. S17. Optimal geometries and calculated molecular frontier orbitals of DYPDMS estimated from density functional theory simulation at B3LYP/6-31G* level.

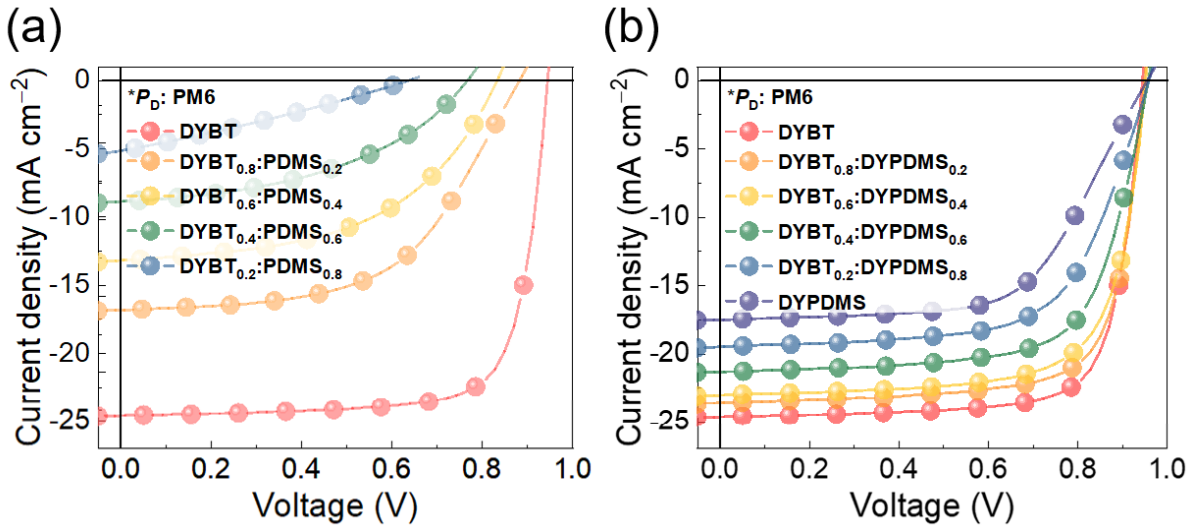

Fig. S18. *J-V* curves of (a) PM6:DYBT:PDMS-based OSCs with varying DYBT:PDMS weight ratios and (b) PM6:DYBT:DYPDMS-based OSCs with varying DYBT:DYPDMS weight ratios.

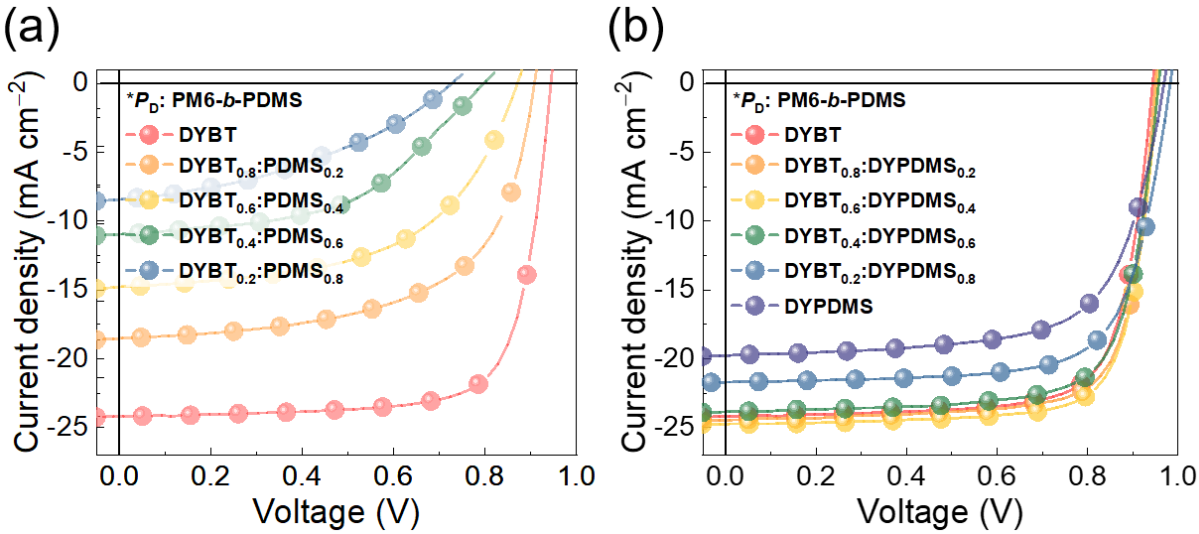

Fig. S19. *J-V* curves of (a) PM6-*b*-PDMS:DYBT:PDMS-based OSCs with varying DYBT:PDMS weight ratios and (b) PM6-*b*-PDMS:DYBT:DYPDMS-based OSCs with varying DYBT:DYPDMS weight ratios.

Table S5. Photovoltaic parameters of PM6:DYBT:PDMS-based OSCs as a function of the DYBT:PDMS weight ratio (averaged from 10 independent devices).

DYBT:PDMS (w/w)	V_{oc} (V)	J_{sc} (mA cm^{-2})	FF	PCE_{max} (%)
10:0	0.95 (0.95 ± 0.01)	24.73 (24.25 ± 0.14)	0.76 (0.75 ± 0.01)	17.83 (17.33 ± 0.24)
8:2	0.89 (0.89 ± 0.01)	16.42 (15.02 ± 0.81)	0.55 (0.54 ± 0.01)	8.25 (7.02 ± 0.54)
6:4	0.84 (0.83 ± 0.01)	13.26 (11.89 ± 0.84)	0.51 (0.50 ± 0.01)	5.65 (4.89 ± 0.51)
4:6	0.77 (0.76 ± 0.01)	8.94 (6.67 ± 1.14)	0.45 (0.43 ± 0.02)	3.07 (2.47 ± 0.80)
2:8	0.64 (0.64 ± 0.01)	5.22 (4.12 ± 1.01)	0.28 (0.26 ± 0.02)	0.95 (0.64 ± 0.44)

Table S6. Photovoltaic parameters of PM6:DYBT:DYPDMS-based OSCs as a function of the DYBT:DYPDMS weight ratio (averaged from 10 independent devices).

DYBT:DYPDMS (w/w)	V_{oc} (V)	J_{sc} (mA cm^{-2})	FF	PCE_{max} (%)
10:0	0.95 (0.95 ± 0.01)	24.73 (24.25 ± 0.14)	0.76 (0.75 ± 0.01)	17.83 (17.33 ± 0.24)
8:2	0.95 (0.95 ± 0.00)	23.69 (23.18 ± 0.26)	0.74 (0.73 ± 0.01)	16.72 (16.28 ± 0.31)
6:4	0.95 (0.95 ± 0.01)	23.13 (22.56 ± 0.18)	0.72 (0.72 ± 0.01)	15.89 (15.56 ± 0.28)
4:6	0.96 (0.95 ± 0.01)	21.42 (21.04 ± 0.22)	0.69 (0.68 ± 0.01)	14.24 (13.89 ± 0.23)
2:8	0.96 (0.96 ± 0.00)	19.58 (19.18 ± 0.31)	0.64 (0.63 ± 0.01)	12.10 (11.83 ± 0.27)
0:10	0.96 (0.96 ± 0.01)	17.60 (17.41 ± 0.17)	0.61 (0.60 ± 0.01)	10.27 (9.90 ± 0.19)

Table S7. Photovoltaic parameters of PM6-*b*-PDMS:DYBT:PDMS-based OSCs as a function of the DYBT:PDMS weight ratio (averaged from 10 independent devices).

DYBT:PDMS (w/w)	V_{oc} (V)	J_{sc} (mA cm^{-2})	FF	PCE_{max} (%)
10:0	0.95 (0.95 ± 0.00)	24.23 (23.50 ± 0.20)	0.75 (0.75 ± 0.01)	17.26 (16.76 ± 0.25)
8:2	0.91 (0.91 ± 0.01)	18.62 (17.38 ± 0.73)	0.60 (0.59 ± 0.01)	10.24 (9.50 ± 0.52)
6:4	0.87 (0.86 ± 0.01)	14.87 (13.14 ± 0.88)	0.55 (0.53 ± 0.02)	7.74 (6.84 ± 0.80)
4:6	0.80 (0.79 ± 0.01)	11.03 (10.17 ± 0.51)	0.49 (0.48 ± 0.01)	4.38 (3.81 ± 0.47)
2:8	0.73 (0.71 ± 0.02)	8.51 (7.64 ± 0.86)	0.38 (0.36 ± 0.02)	2.39 (1.88 ± 0.92)

Table S8. Photovoltaic parameters of PM6-*b*-PDMS:DYBT:DYPDMS-based OSCs as a function of the DYBT:DYPDMS weight ratio (averaged from 10 independent devices).

DYBT:DYPDMS (w/w)	V_{oc} (V)	J_{sc} (mA cm^{-2})	FF	PCE_{max} (%)
10:0	0.95 (0.95 ± 0.00)	24.23 (23.50 ± 0.20)	0.75 (0.75 ± 0.01)	17.26 (16.76 ± 0.25)
8:2	0.95 (0.95 ± 0.01)	24.56 (23.97 ± 0.31)	0.76 (0.75 ± 0.01)	17.84 (17.18 ± 0.28)
6:4	0.96 (0.96 ± 0.01)	24.84 (24.18 ± 0.26)	0.77 (0.76 ± 0.01)	18.28 (17.81 ± 0.23)
4:6	0.96 (0.96 ± 0.00)	23.96 (23.26 ± 0.29)	0.74 (0.73 ± 0.01)	17.09 (16.30 ± 0.35)
2:8	0.96 (0.96 ± 0.01)	21.78 (21.07 ± 0.34)	0.72 (0.71 ± 0.01)	15.07 (14.36 ± 0.32)
0:10	0.97 (0.97 ± 0.01)	19.87 (19.48 ± 0.21)	0.68 (0.67 ± 0.01)	13.08 (12.66 ± 0.19)

Table S9. SCLC charge mobility of photoactive materials.

Material	μ^{SCLC} [a] ($cm^2\ V^{-1}\ s^{-1}$)
PM6	4.4×10^{-4} [b]
PM6-*b*-PDMS	4.7×10^{-4} [b]
DYBT	3.8×10^{-4} [c]
DYPDMS	0.6×10^{-4} [c]

[a]Averaged values from 3 independent samples. [b]Hole and [c]electron mobility.

Table S10. SCLC charge mobility of PM6:acceptors- and PM6-*b*-PDMS:acceptors-based blend films.

P_D	Acceptor	μ_h [a] ($cm^2\ V^{-1}\ s^{-1}$)	μ_e [a] ($cm^2\ V^{-1}\ s^{-1}$)
PM6	**DYBT**	4.0×10^{-4}	3.6×10^{-4}
	DYBT:PDMS	6.1×10^{-5}	2.8×10^{-5}
	DYBT:DYPDMS	3.1×10^{-4}	1.2×10^{-4}
PM6-*b*-PDMS	**DYBT**	4.6×10^{-4}	3.1×10^{-4}
	DYBT:PDMS	8.7×10^{-5}	4.4×10^{-5}
	DYBT:DYPDMS	4.4×10^{-4}	2.8×10^{-4}

[a]Averaged values from 3 independent samples.

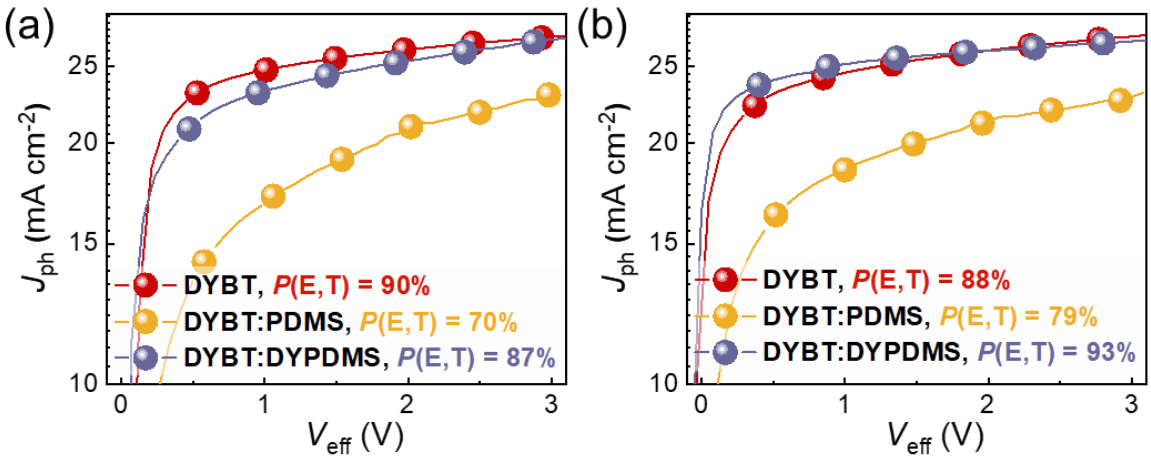

Fig. S20. J_{ph} vs. V_{eff} curves of the (a) PM6:acceptors- and (b) PM6-*b*-PDMS:acceptors-based OSCs.

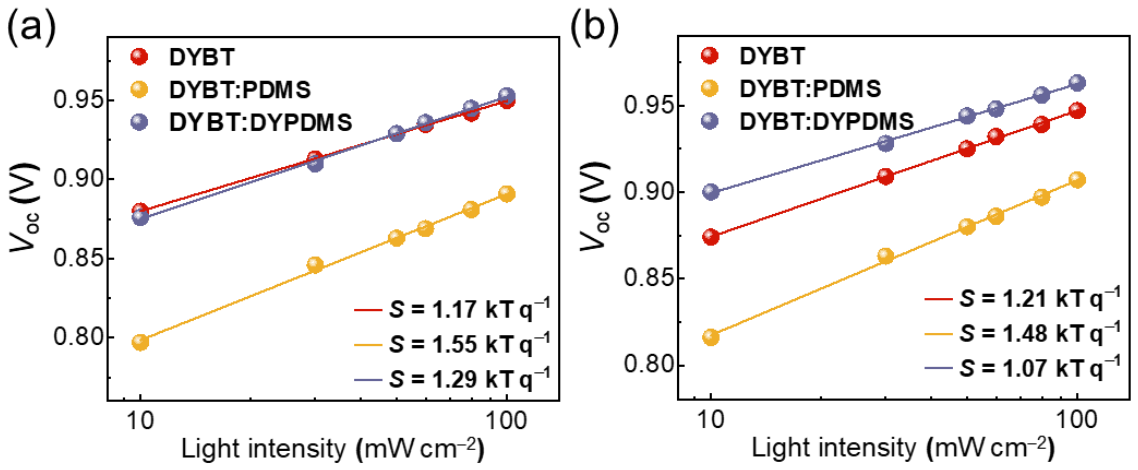

Fig. S21. Light intensity dependent V_{oc} plots of the (a) PM6:acceptors- and (b) PM6-*b*-PDMS:acceptors-based OSCs.

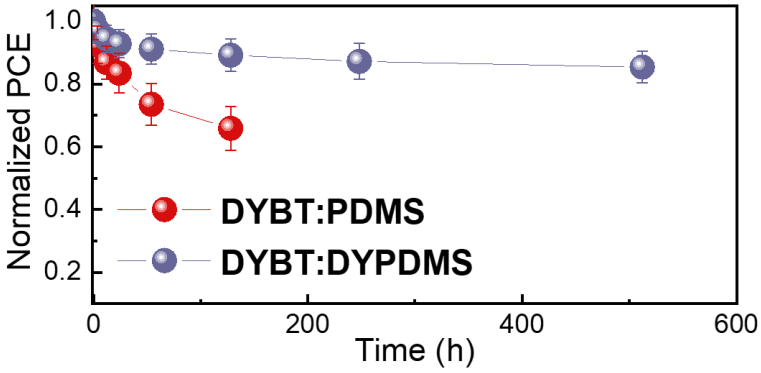

Fig. S22. Thermal stability of the PM6-*b*-PDMS:acceptors-based OSCs under 80 °C.

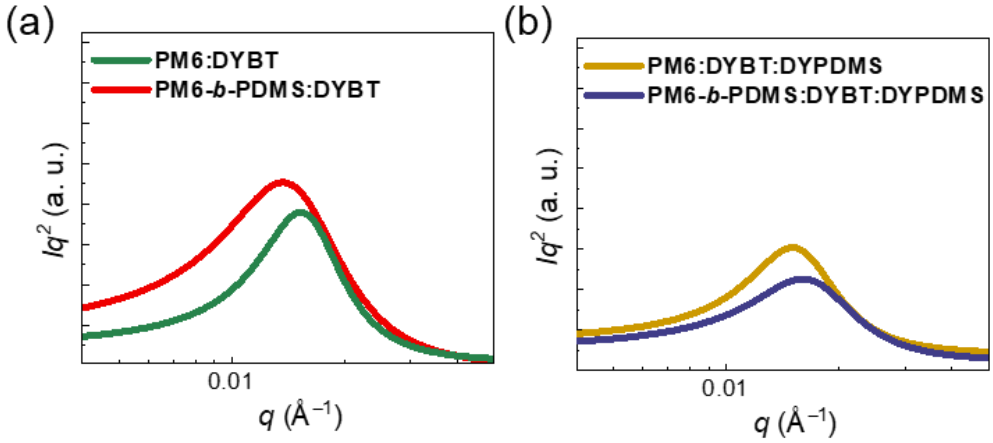

Fig. S23. Lorentz-corrected RSoXS profiles of (a) *P*DS:DYBT and (b) *P*DS:DYPDMS blend films.

Table S11. Morphological parameters of *P*DS:acceptors blend films.

Acceptor	P_D	*r*-DP[a]	d_{RsoXS}[a] (nm)
DYBT	**PM6**	0.68	39
	PM6-*b*-PDMS	0.74	46
DYBT:DYPDMS	**PM6**	0.64	43
	PM6-*b*-PDMS	0.61	38

Estimated from [a]RSoXS profiles.

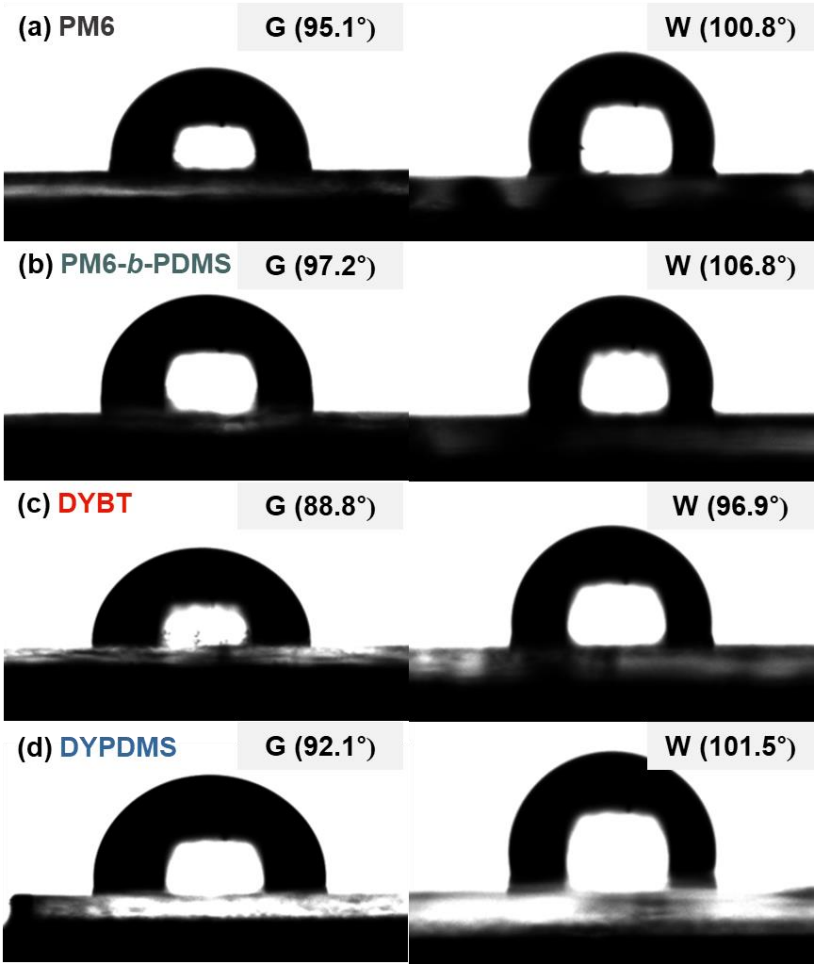

Fig. S24. Contact angles of water (W) and glycerol (G) droplets on the film surfaces of pristine constituents.

Table S12. Contact angle, surface tension, and interfacial tension values obtained from the contact-angle measurement.

Material	Θ_{water} (deg)	$\Theta_{glycerol}$ (deg)	γ^{PM6} (mN m^{-1})[a]	$\gamma^{PM6\text{-}b\text{-}PDMS}$ (mN m^{-1})[b]
PM6	100.8	95.1	–	0.41
PM6-*b*-PDMS	106.8	97.2	0.41	–
DYBT	96.9	88.8	0.57	1.65
DYPDMS	101.5	92.1	1.67	0.41

[a-b]Interfacial tension with [a]PM6 and [b]PM6-*b*-PDMS.

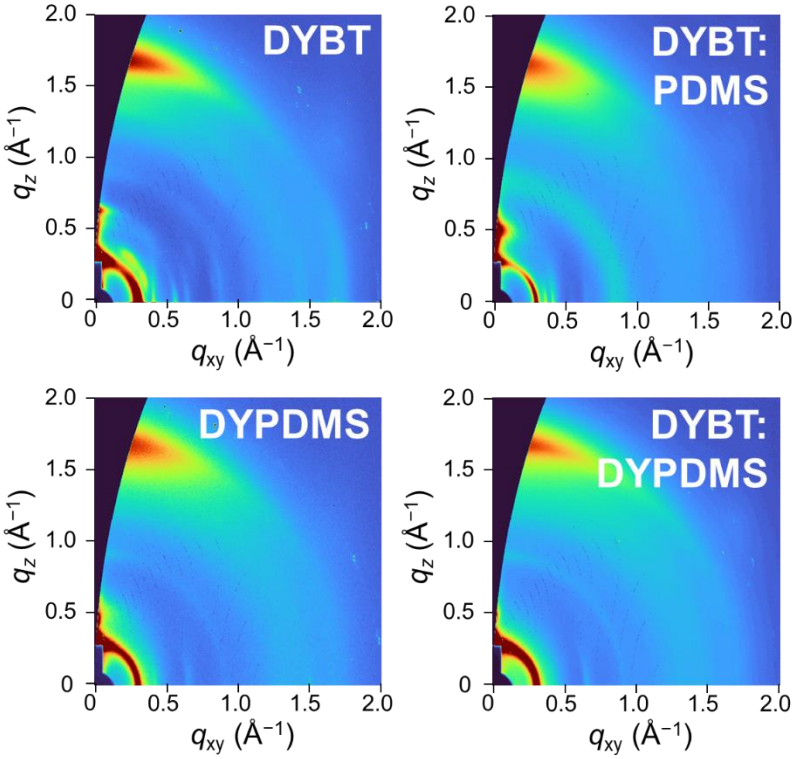

Fig. S25. GIXS 2D-images of the PM6-*b*-PDMS:acceptors blend films.

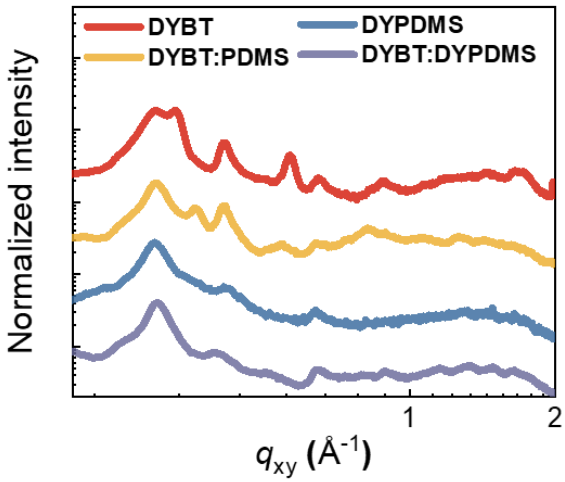

Fig. S26. GIXS linecut profiles in the IP direction of the PM6-*b*-PDMS:acceptors blend films.

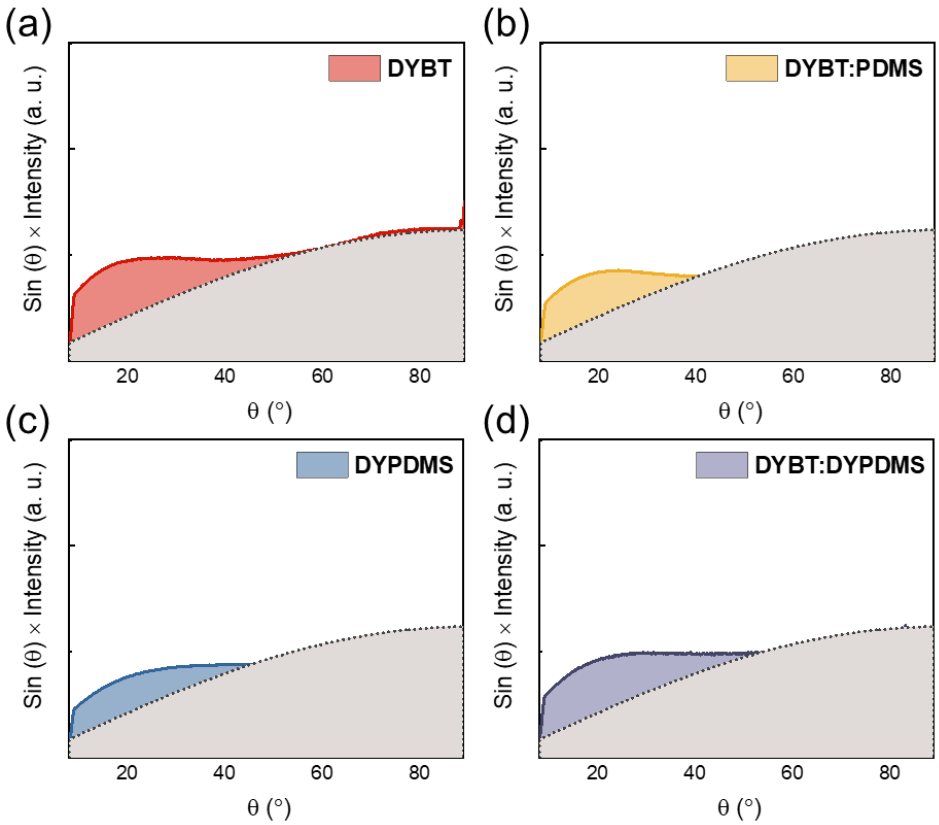

Fig. S27. Pole figures of the PM6-*b*-PDMS:acceptors blend films acquired at (010) scattering peaks using GIXS linecut profiles.

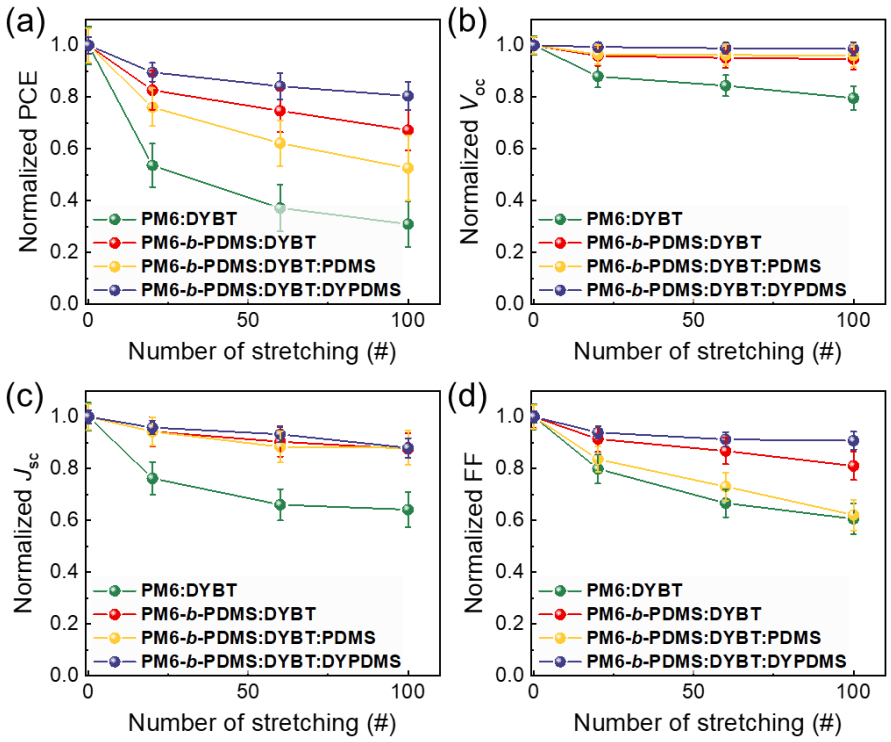

Fig. 28. Normalized (a) PCE, (b) V_{oc}, (c) J_{sc}, and FF of the IS-OSCs after cyclic stretching at 10% strain.

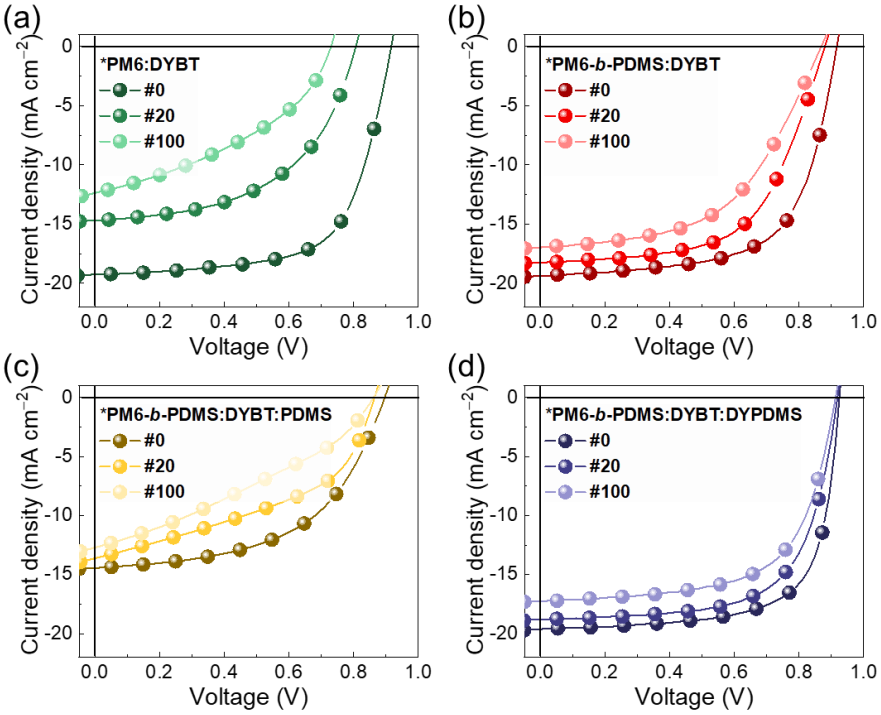

Fig. 29. *J-V* curves of the IS-OSCs based on (a) PM6:DYBT, (b) PM6-*b*-PDMS:DYBT, (c) PM6-*b*-PDMS:DYBT:PDMS, and (d) PM6-*b*-PDMS:DYBT:DYPDMS before and after cyclic stretching at 10% strain.

Table S13. PCE and strain at $PCE_{80\%}$values of IS-OSCs depending on active systems in this study and previously reported studies. (The $PCE_{80\%}$ values were estimated by interpolation of the data reported in the papers.)

Year	Active system	PCE (%)	Strain at PCE_{80} (%)	Ref.
2012	P3HT:PCBM	~1	-	[8]
2013	P3HT:PCBM	0.59	-	[9]
	P3DDT:PCBM	0.29	-	
2016	P3HpT:PCBM	1.25	-	[10]
2017	PTB7-Th: $PC_{71}BM$	2.90	-	[11]
2017	PTB7-Th: PCBM	5.32	8.1	[12]
	PTB7-Th:N2200	2.02	20.2	
2018	PTB7-Th:N2200	2.02	20.2	[13]
	PTB7-Th: ITIC	1.66	10.4	
	PTB7-Th: P(NDI2HD-T)	3.00	15.7	
2019	PTzNTz: $PC_{71}BM$	9.70	7.7	[14]
2021	PBDB-T: PCE10:N2200 (1.2:0.8:1)	6.33	11.2	[15].
2021	PM6:Y7	11.2	12.4	[16]
	PM6:PCBM	5.7	5.1	
	PCE12:N2200	5.0	42.3	
2021	PTB7-Th: IEICO-4F	10.1	12.0	[17]
2022	PM6:Y7	11.16	11.3	[18]
	PM6:Y7:N2200 (1:0.8:0.2)	11.71	19.9	
2022	PhAm5:Y7	12.7	31.6	[19]
2022	PM6:Y6	13.8	9	[20]
	PM6:Y6 + BAC (5wt%)	13.4	20	
2022	PBDB-T:PYBDT	8.54	18.0	[21]
	PBDB-T:PYFS-Ran	8.17	32.1	
	PBDB-T:PYFS-Reg	10.64	36.7	
2022	PM6:BTP-eC9	10.30	11	[22]
	PM6-OEG5: BTP-eC9	11.78	22	

2023	PM7:L8-BO	11.28	16.5	[23]
	PM7- Thy10:L8- BO	13.69	43.1	
2023	PM6-OEG5:BTP-eC9 + P(NDI2OD-T2) 10 wt%	12.18	25	[24]
	PM6-OEG5:BTP-eC9 + P(NDI2OD-TCVT) 10 wt%	12.55	32	
2023	PETTCVT-L:L8-BO	6.3	7	[25]
	PETTCVT-M:L8-BO	8	11	
	PETTCVT-H:L8-BO	10.1	16	
2023	D18:L8-BO	12.77	7	[26]
	$D18_{0.8}$-*r*-$PEHDT_{0.2}$: L8-BO	10.97	18	
	$D18_{0.8}$-*s*-$PEHDT_{0.2}$: L8-BO	14.31	31	
	$D18_{0.8}$: $PEHDT_{0.2}$:L8-BO	11.71	12	
2024	D18:MYT	12.19	8	[27]
	D18:TYT-L	13.1	16	
	D18:TYT-S	14.37	31	
2024	PM6:BTP-eC9	8.2	11	[28]
	PM6: PM6-HD:BTP-eC9	7.12	21	
	PM6:N2200	3.21	31	
	PM6: PM6-HD: N2200	2.28	50	
2024	PM6:Y6	12.8	10	[29]
	PM6:FDY-m-TAT	14.29	20	
2024	PBQx-TF:MYT	12.14	15	[30]
	PBQx-TF:DYBT-C0	13.19	21	
	PBQx-TF:DYBT-C4	14.25	35	
	PBQx-TF:DYBT-C8	12.55	30	
2024	PBQx-TCl:PY-IT: N2200(180k) 10%	10.38	42.1	[31]
	PBQx-TCl:PY-IT: N2200(180k) 20%	12.8	51.3	
	PBQx-TCl:PY-IT: N2200(180k) 30%	10.18	55.5	
	PBQx-TCl:PY-IT: N2200(180k) 50%	7.44	59.6	
	PBQx-TCl:PY-IT:	4.9	67.5	

	N2200(180k) 70% PBQx-TCl:PY-IT :N2200(180k) 100%	**4.25**	**82.3**	
2024	PCE12:PY-EH	9.8	7	[32]
	PCE12:PY-SiO	8.2	12	
2024	PBDB-T:N2200	4.00	34	[33]
	PBDB-T:PCBM	3.41	8	
2025	PM6-b-PDMS: DYBT:DYPDMS	12.74	40	**This study**

References

1. J. Yuan, Y. Zhang, L. Zhou, G. Zhang, H.-L. Yip, T.-K. Lau, X. Lu, C. Zhu, H. Peng, P. A. Johnson, M. Leclerc, Y. Cao, J. Ulanski, Y. Li and Y. Zou, *Joule*, 2019, **3**, 1140-1151.
2. G.-U. Kim, C. Sun, J. S. Park, H. G. Lee, D. Lee, J.-W. Lee, H. J. Kim, S. Cho, Y.-H. Kim, S.-K. Kwon and B. J. Kim, *Adv. Funct. Mater.*, 2021, **31**, 2100870.
3. Y. Li, J. Song, Y. Dong, H. Jin, J. Xin, S. Wang, Y. Cai, L. Jiang, W. Ma, Z. Tang and Y. Sun, *Adv. Mater.*, 2022, **34**, 2110155.
4. J.-W. Lee, C. Sun, S. Lee, D. J. Kim, E. S. Oh, T. N.-L. Phan, T. H.-Q. Nguyen, S. Seo, Z. Tan, M. J. Lee, J.-Y. Lee, X. Bao, T.-S. Kim, C. Lee, Y.-H. Kim and B. J. Kim, *Nano Energy*, 2024, **125**, 109541.
5. S. Seo, J.-W. Lee, D. J. Kim, D. Lee, T. N.-L. Phan, J. Park, Z. Tan, S. Cho, T.-S. Kim and B. J. Kim, *Adv. Mater.*, 2023, **35**, 2300230.
6. Z. Wu, C. Sun, S. Dong, X.-F. Jiang, S. Wu, H. Wu, H.-L. Yip, F. Huang and Y. Cao, *J. Am. Chem. Soc.*, 2016, **138**, 2004-2013.
7. C. Zhang, J. Song, J. Xue, S. Wang, Z. Ge, Y. Man, W. Ma and Y. Sun, *Angew. Chem. Int. Ed.*, 2023, **62**, e202308595.
8. D. J. Lipomi, J. A. Lee, M. Vosgueritchian, B. C. K. Tee, J. A. Bolander and Z. A. Bao, *Chem. Mater.*, 2012, **24**, 373-382.
9. S. Savagatrup, A. S. Makaram, D. J. Burke and D. J. Lipomi, *Adv. Funct. Mater.*, 2014, **24**, 1169-1181.
10. E. J. Sawyer, A. V. Zaretski, A. D. Printz, N. V. de los Santos, A. Bautista-Gutierrez and D. J. Lipomi, *Extreme Mech. Lett.*, 2016, **8**, 78-87.
11. L. Li, J. J. Liang, H. E. Gao, Y. Li, X. F. Niu, X. D. Zhu, Y. Xiong and Q. B. Pei, *ACS Appl. Mater. Interfaces*, 2017, **9**, 40523-40532.
12. Y. Y. Yu, C. H. Chen, C. C. Chueh, C. Y. Chiang, J. H. Hsieh, C. P. Chen and W. C. Chen, *ACS Appl. Mater. Interfaces*, 2017, **9**, 27853-27862.
13. Y. T. Hsieh, J. Y. Chen, S. Fukuta, P. C. Lin, T. Higashihara, C. C. Chueh and W. C. Chen, *ACS Appl. Mater. Interfaces*, 2018, **10**, 21712-21720.
14. Z. Jiang, K. Fukuda, W. C. Huang, S. Park, R. Nur, M. O. G. Nayeem, K. Yu, D. Inoue, M. Saito, H. Kimura, T. Yokota, S. Umezu, D. Hashizume, I. Osaka, K. Takimiya and T. Someya, *Adv. Funct. Mater.*, 2019, **29**, 1808378.
15. Q. L. Zhu, J. W. Xue, L. Zhang, J. L. Wen, B. J. Lin, H. B. Naveed, Z. Z. Bi, J. M. Xin, H. Zhao, C. Zhao, K. Zhou, S. Z. Liu and W. Ma, *Small*, 2021, **17**, 2007011.
16. J. Noh, G. U. Kim, S. Han, S. J. Oh, Y. Jeon, D. Jeong, S. W. Kim, T. S. Kim, B. J. Kim and J. Y. Lee, *ACS Energy Lett*, 2021, **6**, 2512-2518.
17. Z. Y. Wang, M. C. Xu, Z. L. Li, Y. R. Gao, L. Yang, D. Zhang and M. Shao, *Adv. Funct. Mater.*, 2021, **31**, 2103534.
18. J. W. Lee, G. U. Kim, D. J. Kim, Y. Jeon, S. Li, T. S. Kim, J. Y. Lee and B. J. Kim, *Adv. Energy Mater.*, 2022, **12**, 2200887.
19. J. W. Lee, S. Seo, S. W. Lee, G. U. Kim, S. Han, T. N. L. Phan, S. Lee, S. Li, T. S. Kim, J. Y. Lee and B. J. Kim, *Adv. Mater.*, 2022, **34**, 2207544.
20. Z. Y. Wang, D. Zhang, M. C. Xu, J. F. Liu, J. Y. He, L. Yang, Z. L. Li, Y. R. Gao and M. Shao, *Small*, 2022, **18**, 2201589.
21. J. W. Lee, C. Sun, S. W. Lee, G. U. Kim, S. Li, C. Wang, T. S. Kim, Y. H. Kim and B. J. Kim, *Energy Environ. Sci.*, 2022, **15**, 4672-4685.
22. J.-W. Lee, C. Lim, S. W. Lee, Y. Jeon, S. Lee, T. S. Kim, J. Y. Lee and B. J. Kim, *Adv. Energy Mater.*, 2022, **12**, 2202224.

23. Q. Wan, S. Seo, S.-W. Lee, J. Lee, H. Jeon, T.-S. Kim, B. J. Kim and B. C. Thompson, *J. Am. Chem. Soc.*, 2023, **145**, 11914-11920.
24. C. Lim, S. Park, D. J. Kim, J.-W. Lee, J.-S. Park, S. Seo, D. Kim, F. S. Kim, T.-S. Kim and B. J. Kim, *J. Mater. Chem. A*, 2023, **11**, 20031-20042.
25. J.-W. Lee, T. N.-L. Phan, E. S. Oh, H.-G. Lee, T.-S. Kim and B. J. Kim, *Adv. Funct. Mater.*, 2023, **33**, 2305851.
26. J.-W. Lee, H.-G. Lee, E. S. Oh, S.-W. Lee, T. N.-L. Phan, S. Li, T.-S. Kim and B. J. Kim, *Joule*, 2024, **8**, 204-223.
27. J.-W. Lee, C. Sun, J. Lee, D. J. Kim, W. J. Kang, S. Lee, D. Kim, J. Park, T. N.-L. Phan, Z. Tan, F. S. Kim, J.-Y. Lee, X. Bao, T.-S. Kim, Y.-H. Kim and B. J. Kim, *Adv. Energy Mater.*, 2024, **14**, 2303872.
28. X. Li, H. Ke, S. Li, M. Gao, S. Li, J. Yu, H. Xie, K. Zhou, K. Zhang and L. Ye, *Adv. Funct. Mater.*, 2024, **34**, 2400702.
29. Y. Ding, W. A. Memon, D. Zhang, Y. Zhu, S. Xiong, Z. Wang, J. Liu, H. Li, H. Lai, M. Shao and F. He, *Angew. Chem. Int. Ed.*, 2024, **63**, e202403139.
30. J. W. Lee, C. Sun, S. Lee, D. J. Kim, E. S. Oh, T. N. L. Phan, T. H. Q. Nguyen, S. Seo, Z. Tan, M. J. Lee, J. Y. Lee, X. C. Bao, T. S. Kim, C. Lee, Y. H. Kim and B. J. Kim, *Nano Energy*, 2024, **125**, 109541.
31. K. Zhou, D. Han, K. Xian, S. Li, M. Gao, K. Zhang, B. Zhao, X. Li, Y. Chen, Y. Geng and L. Ye, *Energy Environ. Sci.*, 2024, **17**, 5950-5961.
32. J. Y. He, D. Zhang, J. F. Liu, L. Yang, Y. R. Gao and M. Shao, *ACS Appl. Mater. Interfaces*, 2024, **16**, 22294-22302.
33. Z. Wang, D. Zhang, M. Xu, J. Liu, J. He, L. Yang, Z. Li, Y. Gao, Y. Chen, H. Gong, L. Zhao, L.-Y. Zhang and M. Shao, *ACS Mater. Lett.*, 2024, **6**, 1811-1819.